EXPLORATORY RESEARCH

sesar JOINT UNDERTAKING

FlyATM4E

Report on results and assessment of the robustness of eco-efficient aircraft trajectories

Deliverable ID:	**D2.2**
Dissemination Level:	**PU**
Project Acronym:	**FlyATM4E**
Grant:	**891317**
Call:	**H2020-SESAR-2019-2**
Topic:	**SESAR-ER4-05-2019 Environment and Meteorology for ATM**
Consortium Coordinator:	**DLR**
Edition date:	**19/08/2022**
Edition:	**00.02.00**
Template Edition:	**02.00.05**

Authoring & Approval

Authors of the document

Name / Beneficiary	Position / Title	Date
Maximilian Mendiguchia Meuser (TUHH)	WP2 contributor	08/07/2022
Abolfazl Simorgh (UC3M)	WP2 Contributor	08/07/2022
Benjamin Lührs (DLR)	WP2 Contributor	08/07/2022
Florian Linke (DLR)	WP2 Leader	08/07/2022

Reviewers internal to the project

Name / Beneficiary	Position / Title	Date
Florian Linke (DLR)	WP2 Leader	08/07/2022
Feijia Yin (TUD)	WP3 Leader	08/07/2022

Approved for submission to the SJU By - Representatives of all beneficiaries involved in the project

Name / Beneficiary	Position / Title	Date
Feijia Yin (TUD)	WP3 Leader	08/08/2022
Sigrun Matthes (DLR)	Coordinator/WP1 Leader	08/08/2022
Florian Linke (DLR)	WP2 Leader	08/08/2022
Benjamin Lührs (DLR)	WP2 Contributor	19/08/2022

Document History

Edition	Date	Status	Name / Beneficiary	Justification
00.00.01	26/03/2022	Initial Draft	Maximilian M. Meuser (TUHH)	New document
00.00.02	29/03/2022	Complete Draft	Maximilian M. Meuser (TUHH)	WP2 internal review
00.00.10	31/03/2022	Submitted Draft	Maximilian M. Meuser (TUHH)	Reviewed document
00.00.12	08/07/2022	Complete Report	Maximilian M. Meuser (TUHH)	Internal review
00.01.00	08/07/2022	Submitted Report	Maximilian M. Meuser (TUHH)	Final version
00.01.01	16/08/2022	Updated Report	Maximilian M. Meuser (TUHH)	SJU comments
00.02.00	19/08/2022	Submitted Report	Maximilian M. Meuser (TUHH)	Reviewed document

EUROPEAN PARTNERSHIP

Co-funded by the European Union

FlyATM4E

FLYING AIR TRAFFIC MANAGEMENT FOR THE BENEFIT OF ENVIRONMENT AND CLIMATE

This Report is part of project that has received funding from the SESAR Joint Undertaking (JU) under grant agreement No 891317 under European Union's Horizon 2020 research and innovation programme.

Abstract

This deliverable describes the integration of uncertainties with regard to climate impact modelling into the existing trajectory optimisation tools Robust optimization of structured airspace (ROOST) and Trajectory Optimisation Module (TOM). Specific adaptations of the trajectory optimisation models are required to consider uncertainties with respect to meteorology and climate impact and the robustness concept developed in FlyATM4E. Flight trajectories from the previously selected traffic scenario are optimised taking into account combinations of individual uncertainties. Furthermore, the spread of the mitigation efficiency of these optimised eco-efficient trajectories is estimated. Finally a robustness assessment is performed based on the results achieved optimising an example set of routes and in a consolidated manner for the entire traffic scenario.

The achievements documented in this deliverable contribute to the overall project objective O2 on the investigation of aviation's climate impact mitigation potential by developing robust flight planning algorithms through the integration of uncertainties from the climate impact analysis and ensemble weather forecasts in ATM.

EUROPEAN PARTNERSHIP

Co-funded by the European Union

Table of contents

EUROPEAN PARTNERSHIP

Co-funded by the European Union

List of Tables

List of Figures

EUROPEAN PARTNERSHIP

Co-funded by the European Union

EUROPEAN PARTNERSHIP

Co-funded by the European Union

List of Acronyms

Acronym	Definition
aCCF	algorithmic Climate Change Function
AIC	Aviation-induced Cloudiness (primarily contrails)
ASK	Available Seat Kilometres

EUROPEAN PARTNERSHIP

Co-funded by the European Union

API	Application Programming Interface
ATR	Average Temperature Response
ARS	Augmented Random Search
BADA	Eurocontrol Base of Aircraft Data
CCF	Climate change function
CDS	Copernicus Climate Data Store
DLR	German Aerospace Centre
ECMWF	European Centre for Medium Range Weather Forecast
EPS	Ensemble Prediction System
ERA5	ECMWF Reanalysis v5
GPOPS	General Purpose Optimal Control Software
GWP	Global Warming Potential
GTP	Global Temperature Potential
IPOPT	Interior Point Optimiser
MARS	Meteorological Archival and Retrieval System
NetCDF	Network Common Data Format
NLP	Nonlinear Programming Problem
OLR	Outgoing Longwave Radiation
PWF	Probabilistic Weather Forecasting
ROOST	Robust Optimisation of Structured Airspace
SID	Standard Instrument Departure Routes
STAR	Standard Arrival Routes
TOM	Trajectory Optimisation Module

EUROPEAN PARTNERSHIP

Co-funded by the European Union

1 Introduction

This report presents and describes the final results obtained within the Work Package 2 (WP2) of the FlyATM4E project towards the optimisation of eco-efficient aircraft trajectories.

The report includes an overview of the background and purpose of this research (Section 1) and a general description of the simulation setup including general assumptions, as well as a summary of the MET-data and the considered traffic scenario (Section 2). The results from the optimisations are presented for each optimisation tool and approach individually in Sections 3.1 and 3.2.. A summary of results followed by the conclusions drawn from these results conclude the report.

1.1 Background

Aviation emissions play a substantial role in the anthropogenic climate change [7]. With an estimated contribution of approximately 3.5% [9], and a historically estimated growth rate of equally 5%[1], the climate impact of aviation has become increasingly relevant.

At the same time, global air transport is expected to grow at rates significantly higher than the annual increases in fuel efficiency. There is thus a risk that the relative contribution of aviation to anthropogenic emissions and the associated climate impact will increase, which is of particular importance due to the special effects of non-CO_2 emissions at high altitudes (formation of contrail cirrus or ozone). These emissions consist mainly of carbon dioxide (CO_2), nitrogen oxides (NO_x), water vapour (H_2O), soot and sulfate aerosols as well as contrails [5]. However, non-CO_2 emissions impact accounts for nearly 2/3 of the total climate impact of aviation, and is highly reliant on atmospheric conditions at the time and location of emission [5].

This geographical and temporal dependency has been previously analysed the in research, e. g. in the REACT4C project, in which the mitigation potential of climate-optimised flight routing as a measure to reduce aviation's climate impact was investigated. Here, the feasibility of adopting flight routes and altitudes leading to a reduced impact of emissions was assessed, and the global effects of such measures were estimated for the North Atlantic flight corridor [3]. By using 4-D climate change functions to assess the climate impact, and combining them with traditional operating cost functions used by airlines, so-called Pareto-fronts could be calculated to determine not only climate-optimal but also cost-efficient flight routes.

In the WeCare project conducted by the German Aero Space Centre (DLR) until 2017, the effects of non-CO_2 emissions and their atmospheric dependencies were investigated. In a feasibility study performed within the ATM4E project, a modelling chain of climate-optimisation was developed and applied to the European Airspace, which introduced the concept of algorithmic climate change functions [20], publishing initial estimates on mitigation potentials on individual trajectories and influence of individual physical climate metrics [14]. Mainly, the cost-benefit potential of climate-

[1] https://www.icao.int/sustainability/Documents/LTF_Charts-Results_2018edition.pdf

EUROPEAN PARTNERSHIP

Co-funded by the European Union

optimised flight trajectories, derived from tactical, weather-dependent optimisation as well as strategic, climatological optimisation of the flight altitude was addressed in order to determine which strategies are most suitable [10].

This analysis, and especially the estimation of eco-efficient trajectories, requires the availability of climate change functions that enable the quantification of the climate impact of emissions as a function of emission location and time. In the course of FlyATM4E, the algorithmic Climate Change Functions (aCCFs) derived and revised from the previous ATM4E project are used [17]. These aCCFs are applied to estimate the climate impact of aviation's emissions, representing one part of the objective functions for the optimisation models. These functions rely on mathematical algorithms to derive the climate impact directly from meteorological forecast data which is available at the flight planning stage.

In WP2 of FlyATM4E, two main contributions take place which will advance the knowledge beyond the state of the art. Firstly, the consideration of uncertainties resulting from (incomplete) representation of climate impact mechanisms and limited forecast quality by integration of forecast uncertainties into the trajectory optimisation process. Secondly, the identification of robust climate-optimised trajectories relying on operationally available MET data (in the form of EPS forecasts), considering uncertainties originating from predictability, future climate development and meteorological variability.

1.2 Purpose

The main goal of this deliverable is to provide an overview of the integration of uncertainties with regard to climate impact modelling into existing trajectory optimisation tools (i.e. Robust optimization of structured airspace (ROOST) and Trajectory Optimisation Module (TOM)). Two different optimisation approaches are applied to flight trajectories taking into account combinations of individual uncertainties. On the basis of these results, an estimation of the spread of the mitigation efficiency of eco-efficient trajectories can be made. Finally, the robustness of these eco-efficient trajectories is assessed.

EUROPEAN PARTNERSHIP

Co-funded by the European Union

2 Simulation setup

Within this section, general assumptions made for both optimisation approaches are presented together with the implemented algorithmic climate change functions in Section 2.1. This includes the integration of uncertainties with regard to climate impact modelling and weather forecast.

The optimisation tools and their individual constraints and conditions follow in Sections 2.2 and 2.3 with an overview and

2.1 General assumptions for all simulations

Within WP2 two different optimisation approaches are implemented to calculate eco-efficient aircraft trajectories. Since the methods implemented in each of them differ, their setup and some of the assumptions made for the optimisations are individual to them. This section presents the general overview of assumptions that apply to both methods.

2.1.1 Implementation of algorithmic climate change functions

Within the project ATM4E, so called algorithmic climate change functions (aCCFs) have been developed for both, CO_2 and non-CO_2 effects. With regard to the non CO_2-effects, ozone and methane (and the resulting Primary Mode Ozone(PMO)) changes from the emission of NO_x, water vapour emissions as well as persistent contrail formation have been considered. The underlying concept was to use detailed calculations of the climate impact (CCFs) and to derive surrogate models from those which only depend on standard meteorological forecast data which is available at the flight planning stage. Consequently, compared to the detailed CCFs, aCCFs allow for a fast-time estimation of the climate impact. Since the aCCFs are based on the CCFs, they inherit the uncertainties associated with the CCFs. Additionally, further uncertainties about the aCCFs arise from the derivation of the aCCFs [17].In the project FlyATM4E, we will rely on a recent updated mathematical formulation of the prototypic aCCFs which is currently under preparation in a scientific article from within the FlyATM4E consortium [19]. In order to assess the robustness of uncertainties originating from the calculation of the climate impact, alternative estimates of aCCFs will be analysed in an additional assessment of climate-optimised trajectories (post-processing) under assumptions using alternative values within the ranges of uncertainty or possible choices and options, as identified in WP1 and handed-over to WP2. With such an approach it will be possible to provide an uncertainty range of, e.g., the climate impact of climate-optimised trajectories, describing the robustness of climate impact mitigation on climate-optimised trajectories.

2.1.2 MET data

The meteorological data necessary to compute the aCCFs is provided by the European Centre for Medium Weather Forecasts. The specific dataset used within FlyATM4E is the ERA5 dataset, which replaces ERA-Interim data used in previous research such as ATM4E. The ERA5 dataset contains hourly estimates (3-hourly for ensemble data assimilations) of a large number of atmospheric climate variables, with different vertical resolution models. Data can be requested via the Copernicus Data Store (CDS) or from the Meteorological Archival and Retrieval System (MARS), which is the Centre's main data archive.

EUROPEAN PARTNERSHIP

Co-funded by the European Union

2.1.3 Traffic scenario

The flight schedule of intra-ECAC flights was obtained from the Sabre Market Intelligence database for 2018. A total of 16,329 routes were identified for the intra-ECAC traffic. Within FlyATM4E, eco-efficient trajectories are computed by optimisation tools, which – depending on the optimisation approach – require large computational effort. This circumstance has been the motivation for finding a way of reducing the complexity of the optimisation problem. A direct approach is to reduce the number of routes to be optimised according to their relative importance for the overall optimisation result. Therefore, all flight routes obtained from the SABRE data base are ranked by their Available Seat Kilometers (ASK) for 2018. As described in D2.1, we will consider the top 100 routes in terms of ASK as a representative subset of data of traffic by total ASK volume and is an efficient first step towards a reduced flight route network. This subset of traffic is the basis for the optimisations performed by ROOST. The optimal control approach used in the TOM (see section 1.1.1) is very intensive in terms of computational effort. Hence, the route network's complexity is required to be reduced substantially. Based on the intra-ECAC flight network, a clustering algorithm has been developed to reduce the complexity of the optimisation problem.

The trajectory planning in FlyATM4E is not intended to be used as a ready-to-use operational solution, but is intended to better understand the relationship between a range of weather situations and associated mitigation potentials, as well as to provide a quantitative estimate on potential mitigation potentials in dedicated weather situations. Implementing these identified potentials will rely on e.g. meteorological classification, in order to identify the adequate mitigation strategy to be implemented in operational flight planning. Within FlyATM4E, many different possible solutions are explored in order to determine the potential of different mitigation strategies. However, in operational flight planning only a reduced number of options might be of importance according to the selected mitigation strategy (e. g. it is not required to determine 100 Pareto optimal solutions per trajectory).

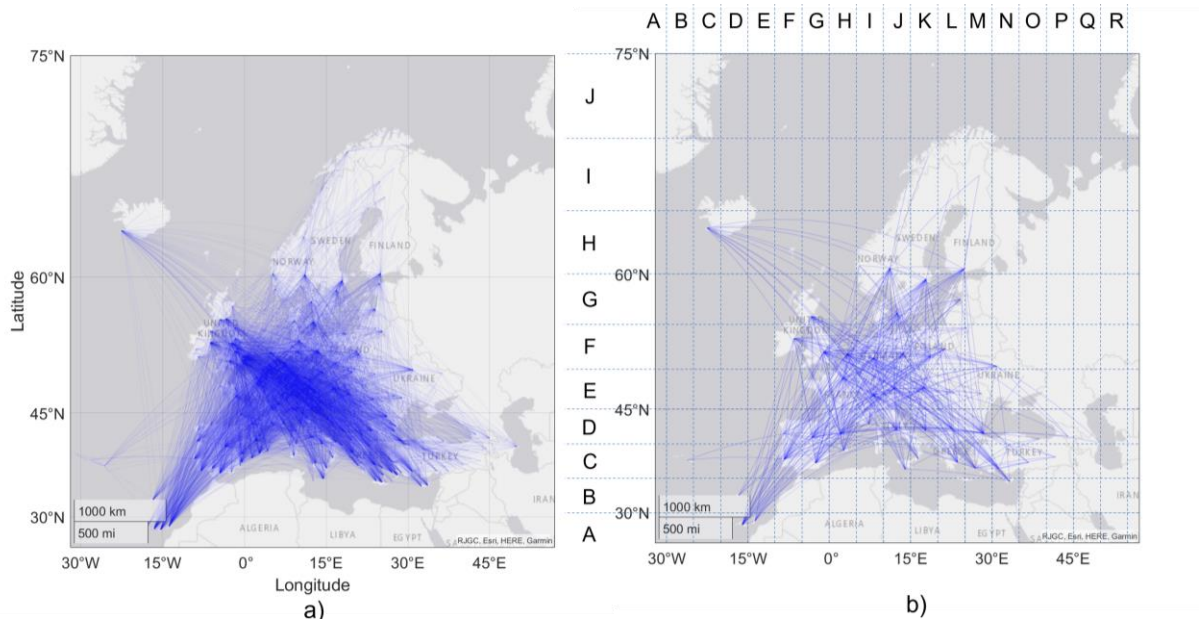

Figure 1: a) Route network of 16,329 origin-destination pairs present in the selected traffic scenario for ECAC-area of 2018. b) Processed fictitious route network with reduced connections located in averaged locations in a 5°- grid weighted by traffic volume.

EUROPEAN PARTNERSHIP
Co-funded by the European Union

2.2 Stochastic flight plan optimization

Robust optimization of structured airspace (ROOST) is a fast graph-based optimization algorithm capable of determining robust aircraft trajectories in the structured airspace considering meteorological uncertainty, characterized by EPS forecast [21] [23].

The concept of robustness that we refer to is the determination of the aircraft trajectory considering all possible realizations of meteorological variables provided within the EPS weather forecast. In other words, instead of planning a trajectory based on one forecast in a deterministic manner, the aim is to determine a trajectory that is optimal considering the overall performance obtained from ensemble forecasts. In this respect, from the operational point of view, the optimized trajectory is tracked as determined, and the effects of meteorological uncertainties are reflected in the variables such as flight time, fuel burn, and climate impacts. As the optimization problem is constrained by the structure of airspace, it is associated with hybrid decision spaces. To account for discrete and continuous decision variables in an integrated manner, the optimization is performed on the space of probability distributions defined over flight plans instead of directly searching for the optimal profile. A heuristic algorithm based on the augmented random search is employed and implemented on graphics processing units to solve the proposed stochastic optimization computationally fast.

2.2.1 Overview

The aircraft trajectory optimization problem within the context of optimal control theory requires the aircraft dynamical model, flight objectives, and physical and operational limitations [22]. The aircraft dynamical model and physical and operational limitations are necessary to determine operationally feasible trajectories within aircraft trajectory optimization, which will be briefly presented in Section 1.1.1. The objective function (in the aircraft trajectory optimization problem) includes mathematically interpreted goals of path planning. A general formulation of the deterministic aircraft trajectory optimization problem in the context of optimal control theory has been stated in detail in our recently published survey [22] (see equation (5) of [22]). Generally, the aim is to find a control policy that minimizes a cost functional while simultaneously satisfying a set of dynamical, path, and boundary constraints. Here, since the aim is to plan robust climate-aware trajectories under meteorological uncertainty, a robust optimal control problem is to be formulated and solved. In the context of optimal control theory, the following general form of the cost functional (or performance index) is considered for robust problems [23]:

$$J = \mathbb{E}\{M(t_0, \mathbf{x}(t_0), t_f, \mathbf{x}(t_f)) + \int_{t_0}^{t_f} L\ (t, \mathbf{x}(t), \mathbf{u}(t), \mathbf{z}(t), \zeta)\mathrm{d}t\} \tag{1}$$

where $M: \mathbb{R} \times \mathbb{R}^{n_x} \times \mathbb{R} \times \mathbb{R}^{n_x} \to \mathbb{R}$ and $L: \mathbb{R} \times \mathbb{R}^{n_x} \times \mathbb{R}^{n_u} \times \mathbb{R}^{n_z}, \mathbb{R}^{n_\zeta} \to \mathbb{R}$ are the Mayer and Lagrange terms called terminal cost and cost-to-go, respectively. n_x, n_u and n_z represent the dimension of state vector $\mathbf{x}(\cdot)$, control vector $\mathbf{u}(\cdot)$ and vector of algebraic variables $\mathbf{z}(\cdot)$ of the dynamical system (e.g., aircraft dynamics for aircraft trajectory optimization problem), respectively. ζ denotes the vector of uncertain variables assumed to have a known probability distribution function (e.g., ensemble weather forecast in this case). The uncertain variables perturb the state, control, and algebraic variables through the system dynamics as $\dot{\mathbf{x}}(t) = \mathbf{f}(t, \mathbf{x}(t), \mathbf{u}(t), \mathbf{z}(t), \zeta)$. The nonlinear function $\mathbf{f}(\cdot)$ is assumed to be a measurable function in ζ.

In the following, we will briefly present the required elements to formulate climate optimal trajectory planning problem.

EUROPEAN PARTNERSHIP

Co-funded by the European Union

2.2.2 Optimization constraints

Generally, three types of constraints are considered for the trajectory optimization problems known as dynamical constraints, path constrain, and boundary constraints.

For ROOST, the following full 4D point-mass model of aircraft is considered as the dynamical constraint allowing to obtain feasible motion of aircraft:

$$\begin{bmatrix} \dot{\phi} \\ \dot{\lambda} \\ \dot{h} \\ \dot{v} \\ \dot{m} \end{bmatrix} = \begin{bmatrix} (v\cos\gamma\cos\chi + w_y)(R_M(\phi) + h)^{-1} \\ (v\cos\gamma\sin\chi + w_x)((R_N(\phi) + h)\cos\phi)^{-1} \\ v\sin\gamma \\ (\mathrm{T}(C_T) - D(C_L))m^{-1} - g\sin\gamma \\ -FF(C_T) \end{bmatrix}$$

where λ is the longitude, ϕ is the latitude, h is the altitude, v is the true airspeed, m is the mass, C_T is the thrust coefficient, γ is the climb angle, χ the heading and $C_L(\gamma) = (2mg\cos\gamma)/(\rho v^2 S)$. In addition, (w_x, w_y) are the components of the wind, R_M and R_N are the Earth's ellipsoid radii of curvature in the meridian and the prime vertical, respectively, T and are the magnitude of the thrust and drag forces, g is the Earth's gravity, FF is the fuel burn rate and S is the wetted surface of the aircraft. BADA model is employed to provide the aerodynamic and propulsive performance of the aircraft. As the trajectory optimization is performed within the structured airspace, the evolutions of aircraft's states are constrained [21, 23]. The following briefly presents our proposed modeling of airspace structure and the flight plan.

The airspace is modeled as a directed acyclic graph $G = (V, E)$, where V represents navigation waypoints connected by airway edges $e \in E$. The trajectory is assumed to start at the end of the departure procedure and ends at the beginning of the arrival procedure to the destination airport, denoted as $o \in V$ and $d \in V$, respectively. We define the flight plan F with a tuple $(R, \overline{\mathrm{FL}}, \overline{\mathrm{M}}, C, D, d_D)$. In the flight plan ($F$), the route (or lateral path) denoted by R includes a sequence of waypoints i.e., $R := (r_0, r_1, \ldots, r_{n_r})$. The vertical profile of the cruise, i.e., $\overline{\mathrm{FL}}$, is composed of an ordered sequence of tuples of the form (r_k, FL_k), indicating that, if the aircraft is in the cruise phase, it will switch to the flight level FL_k when reaching the waypoint r_k (see). The Mach schedule $\overline{\mathrm{M}} := (\mathrm{M}_0, \ldots, \mathrm{M}_{n_r})$ indicates the target Mach number M_k at waypoint r_k, during the cruise phase. The climb and descent profiles $C, D: \mathbb{R} \to \mathbb{R}$ are represented by continuous and piecewise-differentiable functions mapping the altitude to the target airspeed during the climb and descent phases, respectively. Finally, a scalar variable d_D shows the distance-to-go to the destination node at which the aircraft should end the cruise and start the descent phase.

EUROPEAN PARTNERSHIP
Co-funded by the European Union

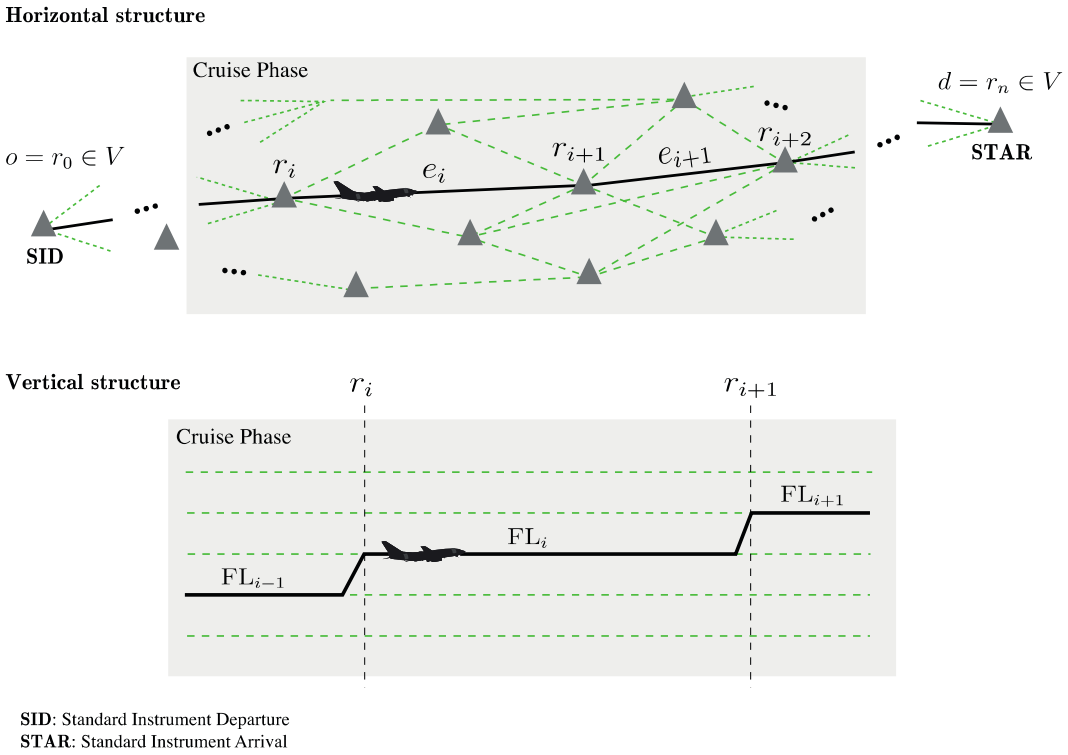

Figure 2. Structure of airspace.

In addition to the dynamical constraint and structure of airspace, a set of path and boundary conditions are required to generate applicable and feasible trajectories. Initial and final values of states such as the geographical location of origin and destination, initial mass, and initial speed are some of the considered boundary conditions. Feasible ranges for speed profile and altitude are examples of the considered path constraints [22].

2.2.3 Cost functional

Within the proposed robust aircraft trajectory optimization, the uncertainty is considered in the weather forecast. To consider climate impact within aircraft trajectory planning, information on the climate impacts of CO_2 and non-CO_2 emissions is necessary and needs to be included in the objective function. For this purpose, we employ the latest version of aCCFs (i.e., V1.1) provided in D1.2. In addition to the climate impact, the operating cost is a crucial aspect that needs to be considered as it is one of the main interests of airliners. In this respect, our objective function is defined as:

$$\text{Objective function (J)} = \psi_{\text{CST}} \cdot Expected \text{ Operating cost} + \psi_{\text{CLM}} \cdot Expected \text{ Climate impact}$$

where ψ_{CST} and ψ_{CLM} are weighting parameters penalizing cost and climate impact, respectively. Such a definition of objective function allows considering both operating cost and climate impact simultaneously as objectives to be minimized. However, a trade-off typically exists between these two objectives determined by selecting the corresponding weighting parameters, i.e., ψ_{CST} and ψ_{CLM}. This objective function is mathematically formulated as:

EUROPEAN PARTNERSHIP
Co-funded by the European Union

$$
\begin{aligned}
J \quad &= \psi_{\text{CST}}[\psi_t \cdot \text{ Exp. Flight time} + \psi_m \cdot \text{Exp. Fuel burnt}] + \psi_{\text{CLM}} \cdot \text{Exp. ATR} \\
&\text{Exp. Flight time: } \mathbb{E}\{\text{FT}\} := \mathbb{E}\{t_f - t_0\} \\
&\text{Exp. Fuel burnt: } \mathbb{E}\{\text{FB}\} := \mathbb{E}\{m_0 - m_f\} \\
&\text{Exp. ATR: } \mathbb{E}\{\text{ATR}\} := \mathbb{E}\{\int_{t_0}^{t_f} \sum_{i=1}^{5} \psi_{\text{ATR},i} \cdot \text{ATR}_i(t, \mathbf{x}(t), \mathbf{u}(t), \zeta)\text{d}t\}
\end{aligned} \tag{2}
$$

for $i \in \{\text{CH}_4, \text{Cont.}, \text{O}_3, \text{H}_2\text{O}, \text{CO}_2\}$:

$$
\begin{aligned}
&\text{ATR}_{\text{O}_3}(t, \mathbf{x}, \mathbf{u}, \zeta) = 10^{-3} \times \text{aCCF}_{\text{O}_3}(t, \mathbf{x}, \zeta) \cdot \dot{m}_{nox}(t) \\
&\text{ATR}_{\text{CH}_4}(t, \mathbf{x}, \mathbf{u}, \zeta) = 10^{-3} \times \text{aCCF}_{\text{CH}_4}(t, \mathbf{x}, \zeta) \cdot \dot{m}_{nox}(t) \\
&\text{ATR}_{\text{Cont.}}(t, \mathbf{x}, \zeta) = 10^{-3} \times \text{aCCF}_{\text{Cont.}}(t, \mathbf{x}, \zeta) \cdot v_{gs}(t) \\
&\text{ATR}_{\text{H}_2\text{O}}(t, \mathbf{x}, \mathbf{u}, \zeta) = \text{aCCF}_{\text{H}_2\text{O}}(t, \mathbf{x}, \zeta) \cdot \dot{m}(t) \\
&\text{ATR}_{\text{CO}_2}(t, \mathbf{x}, \mathbf{u}, \zeta) = \text{aCCF}_{\text{CO}_2} \cdot \dot{m}(t)
\end{aligned}
$$

Where $\mathbf{x}, \mathbf{u}$ are the state and control vectors of aircraft dynamical model [22, 23], ATR_i and aCCF_i are the average temperature response over the next 20 years with business-as-usual (BAU) future emission scenario and the algorithmic climate change function associated with species i, m is flight mass, t is the flight time, v_{gs} is the groundspeed, $\dot{m}_{nox}(t) (= FF(\mathbf{u}, t) \cdot \text{EI}_{\text{NO}_x}(\mathbf{x}, \mathbf{u}, t))$ is the NO_x emission rate in [g(NO_2)/s], $\text{EI}_{\text{NO}_x}(\cdot)$ is the NO_x emission index in [g(NO_2)/kg (fuel)] and FF is the fuel flow in [kg(fuel)/s]. $\text{EI}_{\text{NO}_x}(\cdot)$ is calculated employing modified Boeing Fuel Flow Method 2 [2][8]. t_0 and t_f are the initial flight time and final flight time weighted by ψ_t = 0.75 [USD/s], and m_0 and m_f are the initial mass and final mass weighted by ψ_m = 0.51 [USD/kg] to express operating cost in USD called simple operating cost (SOC) [24]. As can be seen in the formulation of the objective function, the expected operator has been used (i.e., $\mathbb{E}\{.\}$). This is due to the effects of the weather forecast uncertainty on the aircraft trajectory. The forecast-related uncertainties are denoted here with the vector ζ. For instance, the uncertainty in $\text{ATR}_{\text{O}_3}(t, \mathbf{x}, \zeta)$ is due to uncertainty in aircraft trajectories (i.e., aircraft mass $(m(t))$ which is affected by uncertainty in temperature and wind) and also temperature and geopotential for calculating aCCF_{O_3}.

2.2.4 Solution Approach: Probabilistic 4D flight planning in structured airspace

The optimal control problem formulation stated in equation (1) is a general form. Depending on the benchmark problem, some reformulations and approximations are normally made to address the required performances, such as computational complexity. For instance, within the current formulation (i.e., equations (1) and (2)), the decision variable is only the control policy in the continuous domain; however, within some numerical approaches, such as the direct collocation approach, the system's states are also considered as decision variables and represented in a discrete fashion [22]. In this section, we will slightly reformulate the optimal control problem to make it more suited for the proposed path planning problem. The proposed aircraft trajectory optimization is stated by employing the method firstly developed in [21], which is a stochastic optimization technique for the structured airspace and capable of determining an optimized trajectory in four dimensions, i.e., latitude, longitude, altitude, and time. The detailed discreption of methodology for planning robust climate-aware trajectories can be found in [23].

EUROPEAN PARTNERSHIP
Co-funded by the European Union

The goal is to find an optimal flight plan F^o (i.e., $(R^o, \overline{\text{FL}}^o, \overline{\text{M}}^o, C^o, D^o, d_D^o)$, (see Section 1.1.1)) that minimizes the objective function given in equation (2) with respect to some dynamical, path and boundary constraints. For this purpose, as the first step, the performance of any given flight plan needs to be evaluated considering the defined objective function (equation (2)). Then, finding the most optimal flight plan, satisfying the constraints and minimizing the objective function by employing an iterative algorithm.

To determine the performance of a flight plan and evaluate the cost function equation (2), the corresponding trajectories of the aircraft are to be calculated using the aircraft dynamical model. Aircraft trajectories are affected by uncertainty in atmospheric variables, including temperature and wind. The uncertainty in magnitude and direction of the wind will affect groundspeed and, consequently, flight time and fuel burn. In addition, uncertainty in temperature affects fuel burn because the propulsive and aerodynamic performance of the aircraft and also airspeed depend on temperature . From equation (2), one can conclude that the uncertainty in flight time and flight mass can also affect the climate impacts (see). In this study, the uncertainty in meteorological variables represented using ensemble forecasts is considered in the trajectory optimization problem. In the proceeding formulations, the set of required weather variables is denoted as random weather variable W: (T, w_x, w_y,GH,r,q,PVU,OLR), taking discrete values as $\{W_1, W_2 \cdots, W_N\}$, with a probability of $\mathbf{P}(W = W_i) = N^{-1}$, for $i = 1, \cdots, N$. In addition to uncertainty in meteorological variables, the initial flight time and flight mass are also considered with uncertainties, which are modeled as Gaussian variables, i.e., $t_0 \sim N(\bar{t}_0, \sigma_{t_0})$ and $m_0 \sim N(\bar{m}_0, \sigma_{m_0})$, respectively. shows how the uncertainties associated with initial flight conditions and meteorological variables are propagated and affect the efficiency of aircraft trajectory within climate optimal aircraft trajectory planning.

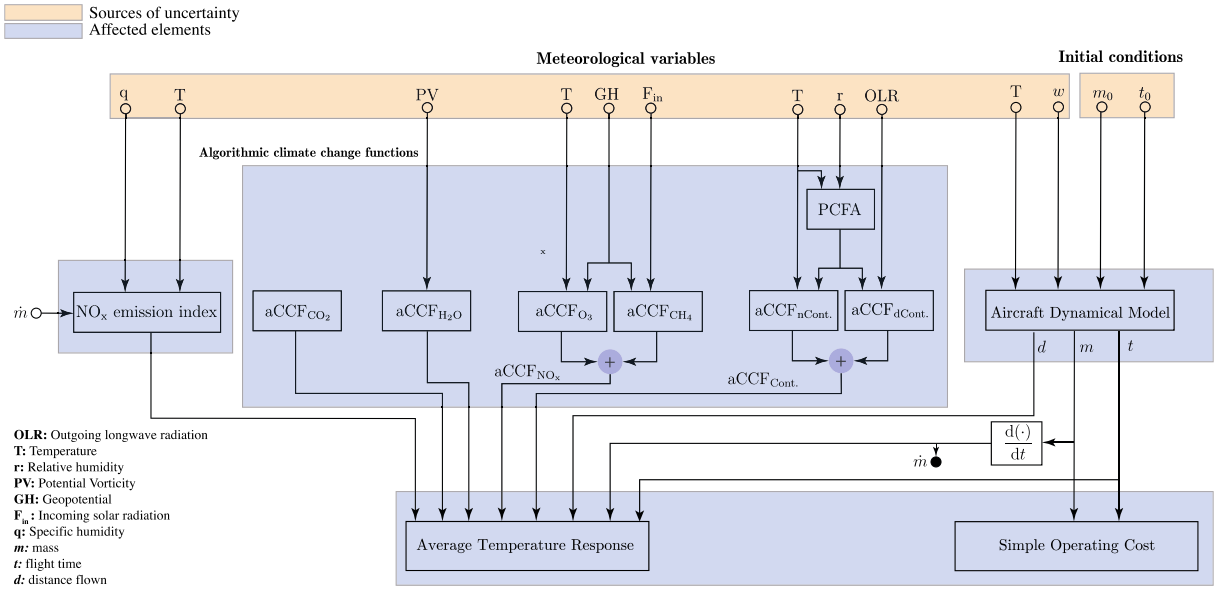

Figure 3. Propagation of the uncertainty (associated with initial flight conditions and meteorological variables) within climate optimal aircraft trajectory planning.

Heun's method [21] is adopted for integrating the aircraft dynamics (i.e., point-mass model) along discretized segment of route for each phase, i.e., climb, descent, and cruise using $(\mathrm{d}t)(\mathrm{d}s)^{-1} = v_{gs}^{-1}$. The expected final mass, final time, and ATR after trajectory integration are then received as

$$[\mathbb{E}\{\text{FT}\},\ \mathbb{E}\{\text{FB}\},\ \mathbb{E}\{\text{ATR}\}] = \mathbb{E}\{\text{TI}(F, W, t_0, m_0)\}$$

EUROPEAN PARTNERSHIP
Co-funded by the European Union

where $\mathrm{TI}(\cdot)$ denotes the integration of system dynamics for a given flight plan, a realization of weather variables, and sampled initial conditions. If we use an unweighted average between all ensemble members, we have

$$[\mathbb{E}\{\mathrm{FT}\},\ \mathbb{E}\{\mathrm{FB}\},\ \mathbb{E}\{\mathrm{ATR}\}] \approx \frac{1}{N_{\mathrm{EPS}}}\sum_{j=1}^{N}\mathrm{TI}\,(F, W_j, t_0^j, m_0^j) \tag{3}$$

where the initial times $t_0^j, m_0^j \sim t_0, m_0$ are sampled independently for each member in Monte Carlo-like fashion and the expected ATR is calculated as

$$\mathbb{E}\{\mathrm{ATR}\} = \frac{1}{N_{\mathrm{EPS}}}\sum_{j=1}^{N_{\mathrm{EPS}}}\mathrm{ATR}^j\,; \qquad \mathrm{ATR}^j = \sum_{i=1}^{5}\mathrm{ATR}_i^j$$

for $i \in \{\mathrm{CH_4}, \mathrm{Cont.}, \mathrm{O_3}, \mathrm{H_2O}, \mathrm{CO_2}\}$. For instance, ATR^j for ozone and contrails can be calculated as

$$\begin{aligned}\mathrm{ATR}_{\mathrm{O_3}}^j &= 10^{-3}\int_{t_0^j}^{t_f^j}\mathrm{aCCF}_{\mathrm{O_3}}^j\,(\mathbf{x}^j(t^j), t^j)\times\overbrace{FF(\mathbf{x}^j(t^j,t^j),\mathbf{u}^j(t^j))\times\mathrm{EI}_{\mathrm{NO_x}}^j(\mathbf{x}^j(t^j),\mathbf{u}^j(t^j,t^j))}^{\dot{m}_{nox}^j(t^j)}\mathrm{d}t^j\\ \mathrm{ATR}_{\mathrm{Cont.}}^j &= 10^{-3}\int_{t_0^j}^{t_f^j}\mathrm{aCCF}_{\mathrm{Cont.}}^j\,(\mathbf{x}^j(t^j), t^j)v_{gs}^j(t^j)\mathrm{d}t^j = 10^{-3}\int_0^{s_f}\mathrm{aCCF}_{\mathrm{Cont.}}^j\,(\mathbf{x}^j(t^j(s)), t^j(s))\mathrm{d}s\end{aligned} \tag{4}$$

where $\mathbf{x}^j(t^j)$ and $\mathbf{u}^j(t^j)$ are the state and control variables of the aircraft considering j-th realization of weather variables and j-th sampled initial conditions, $\mathrm{d}s = v_{gs}^j \cdot \mathrm{d}t^j$, and

$$\begin{aligned}\mathrm{aCCF}_{\mathrm{O_3}}^j(\mathbf{x}^j(t^j), t^j) &:= \mathrm{aCCF}_{O_3}(\mathrm{T}^j(\mathbf{x}^j(t^j), t^j), \mathrm{GH}^j(\mathbf{x}^j(t^j), t^j))\\ \mathrm{aCCF}_{\mathrm{Cont.}}^j(\mathbf{x}^j(t^j), t^j) &:= \mathrm{aCCF}_{\mathrm{Cont.}}(\mathrm{T}^j(\mathbf{x}^j(t^j), t^j), \mathrm{OLR}^j(\mathbf{x}^j(t^j), t^j), \mathrm{r}^j(\mathbf{x}^j(t^j), t^j))\end{aligned}$$

where the weather variables such as T^j, GH^j are the j-th ensemble member of the EPS weather forecast. As can be seen in equation (4), the climate impacts due to the $\mathrm{NO_x}$ emission depends on the amount of $\mathrm{NO_x}$ emitted in climate sensitive regions, while for contrails, it depends on the distance flown in persistent contrail formation areas. Since the calculations are similar for different members (i.e., for each ensemble member in equation (3) to calculate expected values), parallelization would be beneficial in reducing computational time. Here, CUDA, a tool for general-purpose computing on the graphics processing unit, is employed to parallel the computations.

The expected values obtained from equation (3) are for a specific flight plan. By these settings, the cost function equation (2) for this flight plan can be approximately evaluated with the following equation

$$J(F) = \psi_{\mathrm{CST}}[\psi_t \cdot \mathbb{E}\{\mathrm{FT}\} + \psi_m \cdot \mathbb{E}\{\mathrm{FB}\}] + \psi_{\mathrm{CLM}} \cdot \mathbb{E}\{\mathrm{ATR}\}. \tag{5}$$

shows how the expected performance is calculated and evaluated for a given flight plan and ensemble weather forecast. The objective now is to find a flight plan that minimizes equation (5), i.e.,:

$$\min_F J(F) = \psi_{\mathrm{CST}}[\psi_t \cdot \mathbb{E}\{\mathrm{FT}\} + \psi_m \cdot \mathbb{E}\{\mathrm{FB}\}] + \psi_{\mathrm{CLM}} \cdot \mathbb{E}\{\mathrm{ATR}\}$$

Since the flight plan includes both discrete and continuous decision variables, the optimizer should be capable of solving the optimization within the hybrid decision spaces. A classical approach to solving

EUROPEAN PARTNERSHIP
Co-funded by the European Union

such optimization problems is mixed-integer nonlinear programming, which is mathematically complex and computationally intensive.

To account for discrete and continuous decision variables in an integrated manner, the optimization is performed on the space of probability distributions defined over flight plans instead of directly searching for the optimal profile. Then, the probability distribution over flight plans is parameterized, allowing to generate multiple flight plans stochastically. The augmented random search algorithm is employed and implemented on GPUs to deliver a near-optimal solution to the resulting stochastic optimization in seconds. The detailed explantion of the approach and implementation are provided in [21,23].

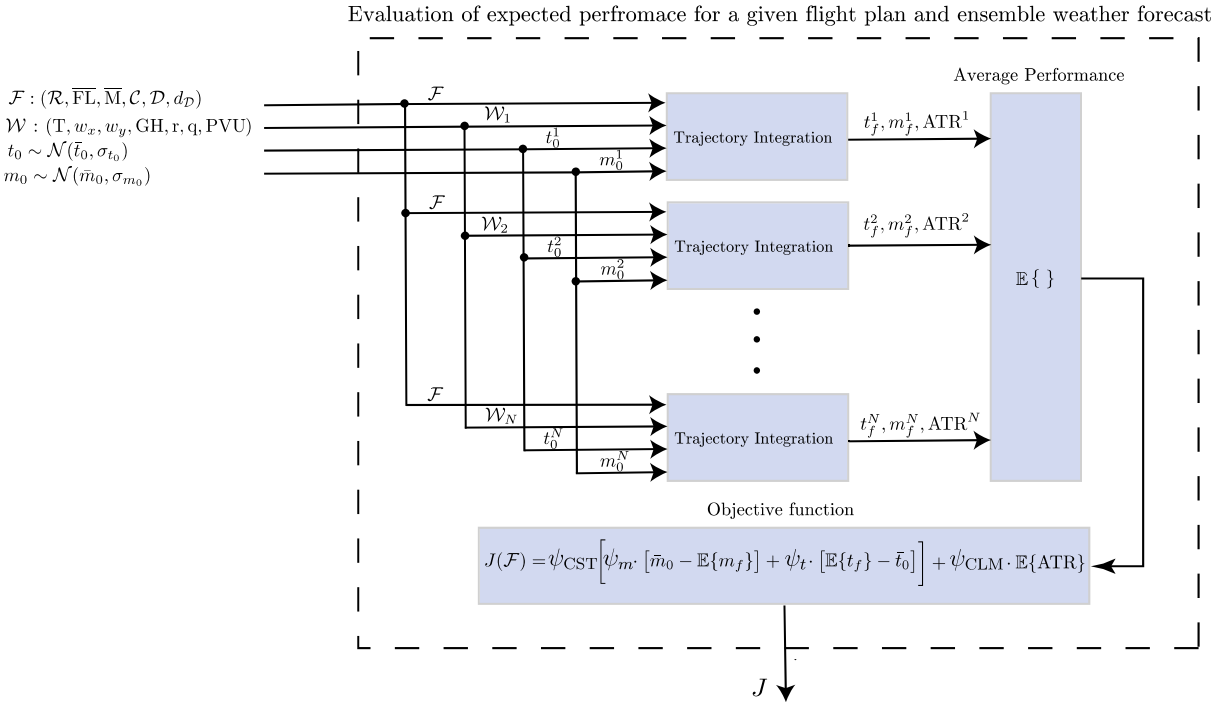

Figure 4. Calculation and evaluation of the expected performance for a given flight plan and ensemble weather forecast.

2.3 Continuous optimal control approach

The Trajectory Optimisation Module (TOM) is an optimisation tool based on an optimal control approach. The workflow applied in the course of WP2 is illustrated in . All simulations are controlled with a process control in which the route, the aircraft, the engine as well as atmospheric conditions are selected. Based on the inputs within the control script, several inputs are loaded, e.g. performance data, emission characteristics, atmospheric data as well as climate impact information and cost models. These serve as input for the optimal control problem which consists of the optimization problem boundary conditions (e.g. flight envelope constraints), the dynamic behaviour of the optimization problem (e.g. equations of motion) as well as the objective function (e.g. costs, climate impact). Finally the problem is solved using an optimal control problem solver.

EUROPEAN PARTNERSHIP
Co-funded by the European Union

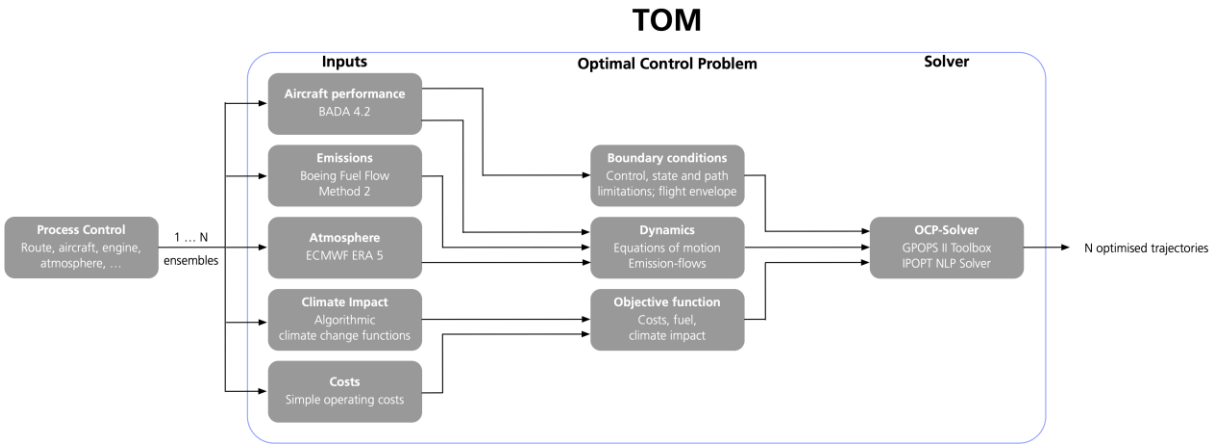

Figure 5. Workflow of the Trajectory Optimization Module (TOM)

In the following, the general optimal control problem formulation is described (see section 1.1.1). Then the control, state, path and event vectors of the optimization problem are defined (see section 1.1.1). The chosen cost functional is explicated in section 1.1.1. Finally, dynamic constraints (see section 1.1.1) and the solving of the optimization problem are presented (see section 1.1.1).

2.3.1 General optimal control problem

The Trajectory Optimization Module relies on an optimal control approach [11]. Hence, the aircraft's motion is described as a vector of state variables $\boldsymbol{x}(t)$ which can be influenced by a vector of control variables $\boldsymbol{u}(t)$. A trajectory is considered optimal, if the temporal development of the control variables $\boldsymbol{u}(t)$ leads to a minimization of the cost functional J as defined in equation while both, the dynamic constraints according to equation as well as the boundary conditions of the state and control variables (equations to) are fulfilled. Further adaptations of the optimization problem can be implemented by additional regulations of a path vector $\boldsymbol{p}(t)$ as shown in equation . Additionally, event constraints can be used in order to define further initial and final boundary values for variables which are not considered as state variables (equations and).

$$J = c_{\Upsilon} \cdot \Upsilon\left(t_0, t_f, \boldsymbol{x}(t_0), \boldsymbol{x}(t_f)\right) + c_{\Psi} \cdot \int_{t_0}^{t_f} \Psi(\boldsymbol{x}(t), \boldsymbol{u}(t), t)\mathrm{d}t \tag{2}$$

$$\dot{\boldsymbol{x}}(t) = f((\boldsymbol{x}(t), \boldsymbol{u}(t), t)) \tag{3}$$

$$\boldsymbol{x}(t_0) \in [\boldsymbol{x}_{min,0}; \boldsymbol{x}_{max,0}] \tag{4}$$

$$\boldsymbol{x}(t_f) \in [\boldsymbol{x}_{min,f}; \boldsymbol{x}_{max,f}] \tag{5}$$

$$\boldsymbol{x}(t) \in [\boldsymbol{x}_{min}; \boldsymbol{x}_{max}] \tag{6}$$

$$\boldsymbol{u}(t) \in [\boldsymbol{u}_{min}; \boldsymbol{u}_{max}] \tag{7}$$

$$\boldsymbol{p}(t) \in [\boldsymbol{p}_{min}; \boldsymbol{p}_{max}] \tag{8}$$

$$\boldsymbol{e}(t_0) \in [\boldsymbol{e}_{min,0}; \boldsymbol{e}_{max,0}] \tag{9}$$

$$\boldsymbol{e}(t_f) \in [\boldsymbol{e}_{min,f}; \boldsymbol{e}_{max,f}] \tag{10}$$

EUROPEAN PARTNERSHIP
Co-funded by the European Union

2.3.2 Definition of state, control, path and event vectors

The aircraft state vector is defined as $\boldsymbol{x} = [\lambda, \varphi, H, v_{\mathrm{TAS}}, m, m_i]^T$. Therein, λ depicts the longitude, φ the latitude, H the flight altitude, v_{TAS} the true airspeed (relative to the air) and m the aircraft mass. The accumulated masses of the engine emissions are denoted by m_i ($i \in \mathrm{CO_2}, \mathrm{H_2O}, \mathrm{NO_x}$).

In order to change the aircraft motion, the control vector $\boldsymbol{u} = [\chi_{\mathrm{H}}, \dot{v}_{\mathrm{TAS}}, \tau]^T$ consists of heading χ_{H}, acceleration $\dot{v}_{\mathrm{TAS}}$ and relative thrust τ (0 for minimum and 1 for maximum thrust).

For the definition of additional constraints, a path vector is defined as $\boldsymbol{p} = [\mathrm{Ma}, v_{\mathrm{CAS}}, c_{L,\mathrm{rel}}]^T$, where Ma represents the Mach number, v_{CAS} the calibrated airspeed and $c_{L,\mathrm{rel}}$ the relative lift coefficient.

Furthermore, the event vector $\boldsymbol{e} = [H_p, v_{\mathrm{CAS}}]^T$ contains the pressure altitude H_p as well as the calibrated airspeed v_{CAS}. The constraints used for the optimization according to equations to are summarized in .

Table 1: Limits of state, control, path and event vectors

Variable	Minimum Value	Maximum Value
Limits of state variables at initial point according to equation		
λ_0	λ_0 [1)]	λ_0 [1)]
φ_0	φ_0 [1)]	φ_0 [1)]
H_0	2,548 m	3,548 m
$v_{\mathrm{TAS},0}$	130 m/s	160 m/s
m_0	m_{ZFW} [2)]+$m_{\mathrm{FOB},0}$ [1)]	m_{TOW} [2)]
$m_{i,0}$	0 kg	0 kg
Limits of state variables at final point according to equation		
λ_f	λ_f [1)]	λ_f [1)]
φ_f	φ_f [1)]	φ_f [1)]
H_f	2,548 m	3,548 m
$v_{\mathrm{TAS},f}$	130 m/s	160 m/s
m_f	m_{ZFW} [2)]+$m_{\mathrm{FOB,f}}$ [1)]	m_{ZFW} [2)]+$m_{\mathrm{FOB,f}}$ [1)]
$m_{i,f}$	0 kg	10^7 kg

Variable	Minimum Value	Maximum Value
General limits of state variables according to equation		
λ	-40°	70°
φ	20°	90°

EUROPEAN PARTNERSHIP

Co-funded by the European Union

H	2,500 m	13,500 m
v_{TAS}	130 m/s	270 m/s
m	m_{ZFW} [2)] + $m_{\mathrm{FOB,f}}$ [1)]	m_{TOW} [2)]
m_i	0 kg	10^7 kg
General limits of control variables according to equation		
χ_{H}	0°	360°
$\dot{v}_{\mathrm{TAS}}$	-2 m/s^2	2 m/s^2
τ	0	1
General limits of path variables according to equation		
Ma	0	$\mathrm{Ma}_{\mathrm{max}}$ [2)]
v_{CAS}	0	$v_{\mathrm{CAS,max}}$ [2)]
$c_{L,\mathrm{rel}}$	0	1
Limits of event variables at initial point according to equation		
$H_{p,0}$	3,048 m	3,048 m
$v_{\mathrm{CAS},0}$	128.61 m/s	128.61 m/s
Limits of event variables at final point according to equation		
$H_{p,f}$	3,048 m	3,048 m
$v_{\mathrm{CAS,f}}$	128.61 m/s	128.61 m/s

[1)] Obtained initial and final latitude and longitude are extracted from the fictitious route network

[2)] Obtained from EUROCONTROL's BADA 4.2 aircraft performance database; m_{ZFW} is estimated assuming a load factor of 0.85, which was the average value for European flights in 2018

2.3.3 Cost functional

For the optimisation with respect to costs and climate impact in the course of FlyATM4E, the cost functional is chosen as formulated in equations and . It is defined as the weighted sum of the simple operating costs (costs are represented as weighted sum of fuel consumption and flight time) and the climate impact expressed as average temperature response (ATR) over 20 years which is represented by the algorithmic Climate Change Functions (aCCFs) which have been further developed in the course of WP1. Also, the costs and the resulting climate impact are normalized with respect to the corresponding reference values of the minimum cost trajectory. In order to determine pareto-optimal solutions of the optimisation problem, the weighting factors c_{SOC} and c_{ATR} are varied between 0 and 1.

Within FlyATM4E the weights of costs and climate impact are varied between the two extreme cases (0 and 1) of climate optimal and cost optimal routings in order to explore the full spectrum of possible

EUROPEAN PARTNERSHIP

Co-funded by the European Union

solutions. However, the final choice of the weights is considered to be defined by politics as there exists no single answer or ideal pair of values. For dedicated strategies, we will provide recommendations on how to select suitable weighting factors depending on the use case (e. g. method for the selection of eco efficient trajectories developed in WP3).

$$J = c_{\mathrm{SOC}} \cdot \underbrace{SOC\left(m_0 - m_f, t_f - t_0\right)}_{\text{Simple operating costs}} \cdot SOC_{\mathrm{ref}}^{-1} + \ldots$$

$$\ldots c_{\mathrm{ATR}} \cdot \underbrace{\int_{t_0}^{t_f} \left(\mathrm{aCCF}_{\mathrm{CO_2}} + \mathrm{aCCF}_{\mathrm{H_2O}}\right) \cdot \mathrm{FF} + \left(\mathrm{aCCF}_{\mathrm{O_3}} + \mathrm{aCCF}_{\mathrm{CH_4}}\right) \cdot \mathrm{EI}_{\mathrm{NO_x}} \cdot \mathrm{FF} + \mathrm{aCCF}_{\mathrm{Contrails}} \cdot v_{\mathrm{TAS}} \, \mathrm{d}t}_{\mathrm{ATR}} \cdot \mathrm{ATR}_{\mathrm{ref}}^{-1} \tag{11}$$

$$c_{\mathrm{SOC}} + c_{\mathrm{ATR}} = 1; \quad c_{\mathrm{SOC}}, c_{\mathrm{ATR}} \in [0,1] \tag{12}$$

2.3.4 Dynamic constraints

The dynamic constraints of the optimal control problem are defined by equations to which substantially are based on the equations of motion of a point mass aircraft with variable mass and three degrees of freedom. Assuming a spherical earth with radius R_E, the temporal changes of latitude and longitude can be described by equations and . Here, γ depicts the flight path angle obtained from $\sin\gamma = \dot{H}/v_{\mathrm{TAS}}$.

The vertical speed of the aircraft $\dot{H}$ is estimated based on the total energy model according to equation ; the minimum and maximum thrust ($\mathrm{Th}_{\mathrm{min}}, \mathrm{Th}_{\mathrm{max}}$) as well as the aerodynamic drag D are estimated using the Base of Aircraft Data (BADA) 4.2 aircraft performance models provided by EUROCONTROL [15].

The temporal derivative of the true airspeed v_{TAS} is equal to the linear acceleration $\dot{v}_{\mathrm{TAS}}$ which is serving as control variable (see equation). Additionally, the change of aircraft mass equals the negative fuel flow FF which is also obtained by applying the BADA 4.2 aircraft performance models (see equation). The emission flow rates $\dot{m}_i$ ($i \in \mathrm{CO_2}, \mathrm{H_2O}, \mathrm{NO_x}$) are estimated by multiplying the fuel flow FF with the corresponding emission index EI_i according to equation . Here, $\mathrm{EI}_{\mathrm{CO2}}$ and $\mathrm{EI}_{\mathrm{H2O}}$ are determined assuming a stoichiometric combustion. In contrast, $\mathrm{EI}_{\mathrm{NOx}}$ is calculated using the EUROCONTROL modified Boeing Fuel Flow Method 2 [2][8].

$$\dot{\lambda} = \frac{v_{\mathrm{TAS}} \cdot \cos\gamma \cdot \sin\chi_{\mathrm{H}}}{(R_E + H) \cdot \cos\varphi} \tag{13}$$

$$\dot{\varphi} = \frac{v_{\mathrm{TAS}} \cdot \cos\gamma \cdot \cos\chi_{\mathrm{H}}}{(R_E + H)} \tag{14}$$

$$\dot{H} = \frac{[\tau \cdot (\mathrm{Th}_{\mathrm{max}} - \mathrm{Th}_{\mathrm{min}}) + \mathrm{Th}_{\mathrm{min}} - D] \cdot v_{\mathrm{TAS}}}{m \cdot g} - \frac{v_{\mathrm{TAS}} \cdot \dot{v}_{\mathrm{TAS}}}{g} \tag{15}$$

$$\dot{v}_{\mathrm{TAS}} = \dot{v}_{\mathrm{TAS}} \tag{16}$$

$$\dot{m} = -\mathrm{FF} \tag{17}$$

$$\dot{m}_i = -\mathrm{FF} \cdot \mathrm{EI}_i \tag{18}$$

EUROPEAN PARTNERSHIP
Co-funded by the European Union

2.3.5 Solving the optimal control problem

The resulting optimal control problem which is defined by the cost functional, the dynamic constraints as well as the limitations of control-, state-, path-, and event-vectors (see equations to), is solved using the MATLAB optimal control Toolbox GPOPS II [16]. GPOPS II is based on a direct approach and transforms the continuous optimal control problem into a discrete nonlinear programming problem (NLP). Finally, the NLP is processed by the NLP solver IPOPT [18].

EUROPEAN PARTNERSHIP

Co-funded by the European Union

3 Results

3.1 Stochastic flight plan optimization

The simulation results employing ROOST are presented in two parts: single route analysis and aggregated results of optimizing the top 100 routes. Before presenting the results, we will depict the aCCFs for a specific scenario and discuss the variability in aCCFs due to the variability in atmospheric conditions characterized using EPS.

3.1.1 Uncertainty analysis

The aCCFs for 13th of June 2018, 00:00 am UTC over the European region at pressure level 250 are depicted in . As can be seen, aCCFs provide spatially resolved information on the climate impacts associated with aircraft emissions. To compare the contribution of each species to the total climate impact, we adopt typical transatlantic fleet mean values to unify the units of aCCFs in K/kg(fuel). The approximated conversion factors for NO_x emission and contrails are 13×10^{-3}Kg(NO_2)/Kg(fuel) and $0.16 \times$ Km/Kg(Fuel), respectively. It is clear from the merged aCCF that the contrails have dominant climate effects.

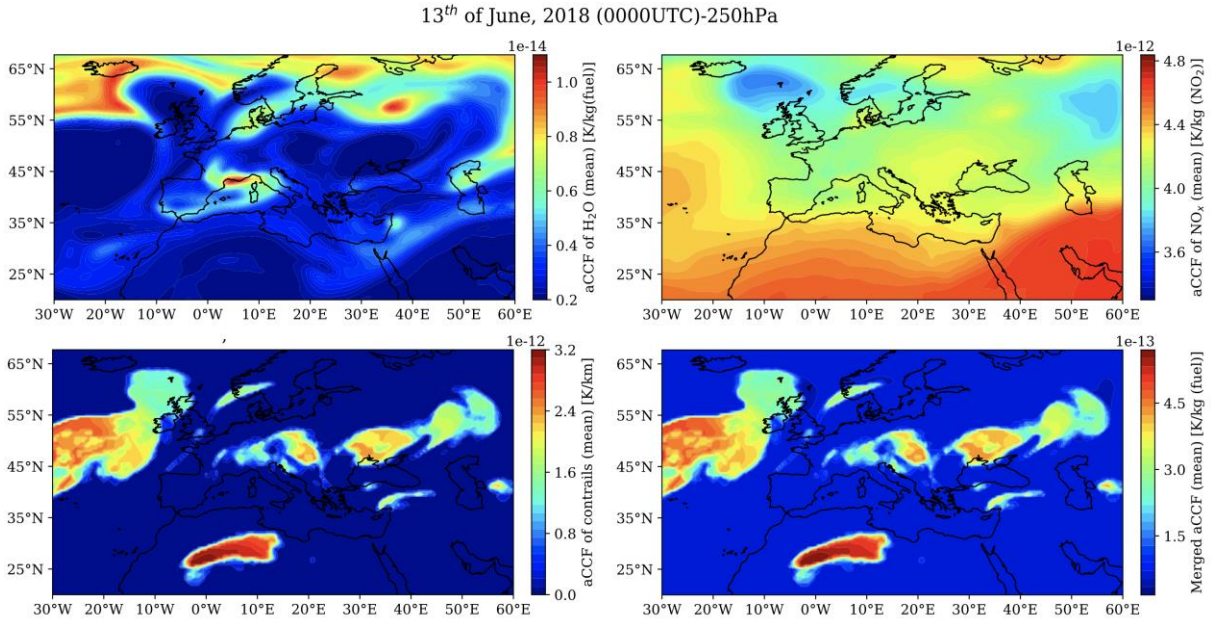

Figure 6. Algorithmic climate change functions on 13th of June 2018, 00:00 am UTC over European region at pressure level 250hPa.

Now, we investigate the effects of variability in atmospheric variables generated using the EPS on the calculated aCCFs. As aCCFs take as inputs meteorological variables, N different aCCFs can be calculated for the EPS weather forecast. For instance, atmospheric variables temperature and relative humidity over ice are required for aCCF of (night-time) contrails. Feeding N probable realizations of these atmospheric variables (i.e., ensemble members), N different aCCFs (i.e., $aCCF_{Cont_i}$ for $i = 1, \cdots, N$) are calculated.

EUROPEAN PARTNERSHIP
Co-funded by the European Union

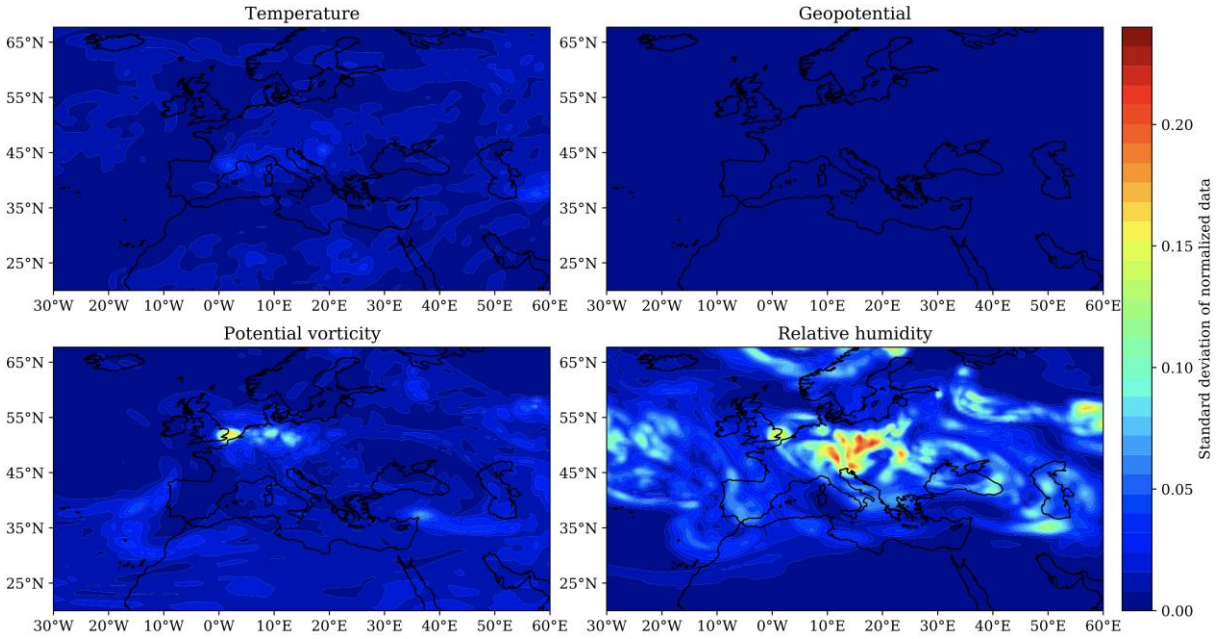

Figure 7. Standard deviation of the normalized weather variables calculated using 10 ensemble members at 250hPa

To investigate the degree of uncertainty (or variability) in the atmospheric variables provided by the EPS and its effects on the computed aCCFs, the standard deviation (STD) is taken from ten ensemble members of the ERA5 reanalysis data products[2]. shows the STD of weather variables required to calculate aCCFs on 13th of June 2018, 00:00 am UTC, at the pressure level of 250hPa. The STD is taken over the normalized variables for comparison purposes. The variability of geopotential and temperature is small compared to potential vorticity and relative humidity. The STDs of the calculated aCCFs based on the ensemble members are illustrated in . Since the aCCF of NO_x emission (i.e., methane, ozone and PMO) depends on geopotential and temperature, its STD is small compared to the aCCFs of water vapor and (night-time) contrails, which are based on potential vorticity and relative humidity, respectively. Notice that the uncertainty in contrails' climate impact is much higher than water vapor due to the variability of relative humidity in satisfying the persistency condition of contrails, called persistent contrail formation areas (PCFA) [23] (see STD of PCFA in). It can be concluded that up to 40% deviation from mean values is probable with the aCCF of contrails. In spite of neglectable uncertainty in the aCCF of NO_x, and also relatively low uncertainty in the aCCF of water vapor compared to aCCF of contrails, due to the dominant climate impact of contrails, the net non-CO_2 climate effect is highly uncertain (see STD of the merged aCCF in), which must be crucially taken into consideration.

[2] https://cds.climate.copernicus.eu/

EUROPEAN PARTNERSHIP
Co-funded by the European Union

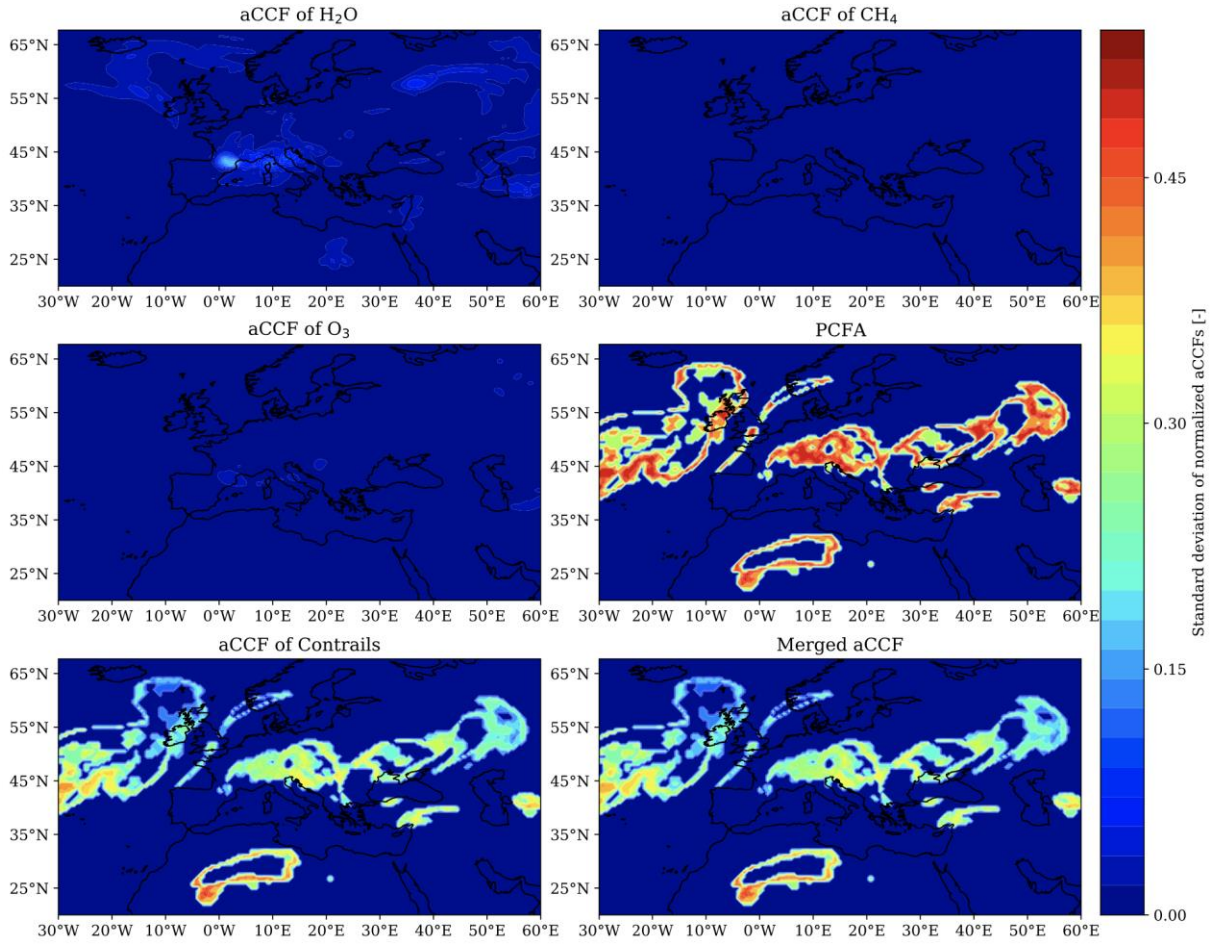

Figure 8. Standard deviation of the normalized aCCFs calculated using 10 ensemble members at 250hPa.

3.1.2 Single Route analysis

The effectiveness of the proposed optimization algorithm to plan robust climate optimal aircraft trajectories with respect to uncertain meteorological conditions is analyzed for a flight from Frankfurt to Kyiv on three different days: on 13th of June 2018, 0000UTC, a scenario in which aircraft flies through areas favorable for the formation of persistent contrails (i.e., warming contrails), 20th of December 2018, 1200UTC, a scenario with cooling contrails, and 10th of December 2018, 1200UTC, a scenario with no formation of persistent contrails. The dominant climate impact of contrails is the main reason for selecting these scenarios, providing better insight into the mitigation potentials.

For the route graph, the full airspace graph of the considered days is filtered and processed to include all paths from the standard instrument departures (SIDs) of the origin airport to the standard instrument arrivals (STARs) of the destination airport with the maximum length of 104% of the shortest path length. The initial flight time and mass are modeled as Gaussian variables: $t_0 \sim N(0000\ \text{UTC}, 10)$[s] and $m_0 \sim N(61600,10)$[kg]. Due to ease of availability, the ERA5 Reanalysis data products containing ten ensemble members are adopted in this study. However, forecast data with more ensemble members can be employed similarly.

The weighting parameters of the objective function given in equation (5) are selected as: $\psi_{\text{CST}} = \alpha$ [-] and $\psi_{\text{CLM}} = (1 - \alpha[-])$K [USD/K]. K is a scaling factor determined as

EUROPEAN PARTNERSHIP
Co-funded by the European Union

$$k = \frac{SOC_{climate} - SOC_{cost}}{ATR_{cost} - ATR_{climate}}$$

where for instance, $SOC_{climate}$ is the SOC calculated when the optimization objective is only the climate impact or ATR_{cost} is the ATR when the objective is only SOC. $\alpha \in [0,1]$ is a weighting parameter that penalizes cost versus climate impact in which $\alpha = 0$ is the pure cost optimal and $\alpha = 1$ is the pure climate optimal routing strategies. In the simulations, we consider five different values for α in order to explore the trade-off between operating cost and climate impact represented respectively by SOC and ATR.

3.1.2.1 Example 1 (Formation of persistent contrails during nighttime)

We consider a scenario in which aircraft flies through warming contrails for the cost optimal routing option. Before presenting the results, the performance of ROOST in terms of convergence and computational time is analyzed.

Since the optimization approach is stochastic, different results may be obtained with different runs. To explore the sensitivity of the optimization method, 50 different runs are performed with similar settings for the pure cost (i.e., $\alpha = 1.0$) and pure climate optimal (i.e., $\alpha = 0.0$) routing options. Then, the objective gap is calculated considering the best performance obtained from different solutions (i.e., the minimum value of J) as the reference. The convergence performances with averaged values as solid lines and 0, 10, 90, and 100 percentiles are depicted in . For both cases, the estimated objective gaps quickly reduce up to 1% of the values of the objective functions J with around 700 iterations ($\approx 2.8s$) for cost and 900 iterations ($\approx 3.6s$) with climate optimal one. As the climate optimal routing option is associated with the inclusion of aCCFs calculated from meteorological variables, the optimization is much more complex, which can be validated in . With around 4000 iterations ($16s$), the objective gap is reduced up to 0.5% of J. Consequently, with a maximum of 4000 iterations, near-optimal performance can be obtained with +0.5% maximum deviation around the best-obtained value (i.e., most optimal case).

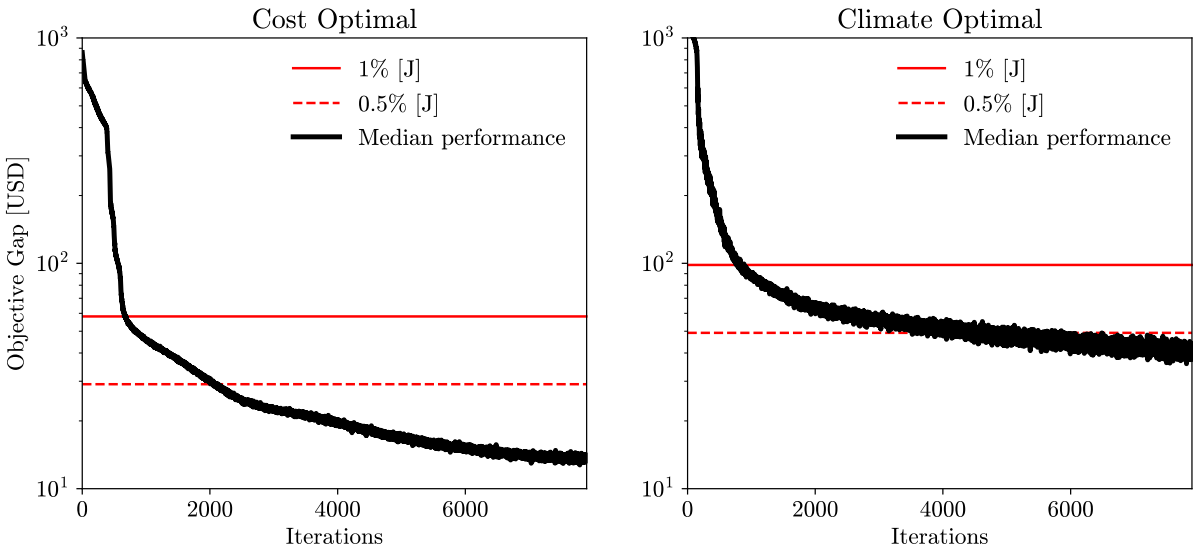

Figure 9. Convergence performance of the optimization approach (1 iterations ≈4 ms).

EUROPEAN PARTNERSHIP
Co-funded by the European Union

Now, we proceed to present the obtained results. The aircraft profiles and climate responses for different routing options are given in Figure 12 and **Figure 13**, respectively. The SOC depends on the flight time and fuel consumption. Therefore, the aircraft for routing strategies with higher values of α, such as $\alpha = 1.0,0.8$, tends to fly at higher altitudes within the vertical constraints because flying at higher altitudes is beneficial to reducing fuel consumption, which contributes a large part of the total operating cost (see). By analyzing the lateral paths depicted in a with the direction and speed of wind at different flight levels, one can see that aircraft deviates from the shortest path to benefit from stronger tailwinds. For trajectories with lower climate impacts, as can be seen in b, the aircraft flies at relatively lower altitudes compared to cost optimal routing options mainly to avoid the formation of persistent contrails (due to warming impacts during nighttime). The climate optimal routing options reduce the warming effects of contrails. Although the warming climate impact of NO_x emission and water vapor increases with the climate optimal trajectories, the net climate impact decreases. This is because the contrails' climate impact outweighs the impact associated with other species. The contribution of each species to total climate impact, variability of obtained climate impacts, and SOC with the ranges of uncertainty and Pareto-frontiers are provided in . For a specific case ($\alpha = 0.2$), by accepting an increase of 4% in cost, there is a potential to mitigate the climate impact by 55% considering mean values. In Section 1.1.1, it was shown that the variability of relative humidity among ensemble members is high, leading to high uncertainty in aCCF of contrails. As expected, the obtained contrails' climate impact is highly uncertain when aircraft flies through areas sensitive to form persistent contrails. In contrast, as the aircraft tends to avoid PCFA, the ranges of uncertainty reduce, in which, for the complete avoidance that is achieved with $\alpha = 0.0$, the climate impact is almost deterministic. In addition, SOC requires flight time and fuel burnt to represent operating cost in USD, and as it is affected by relatively less uncertain atmospheric variables wind and temperature (compared to relative humidity) for the considered case study (analyzed in Section 1.1.1), the uncertainty in its value is small.

By analyzing the contribution of each species to the net ATR for different α's, one can conclude that **the mitigation potential is achieved mainly by avoiding contrails sensitive areas**, which result in slight increases NO_x emission a. However, **when the contrails are completely avoided ($\alpha = 0.2$), the optimizer tends to reduce NO_x emission** mainly by reducing speed to reduce the fuel flow required to calculate NO_x emission index and also total NO_x emission (i.e., NO_x emission = NO_x emission index * fuel burnt). Reducing NO_x emission due to flying at lower speed is achieved at the expense of a considerable increase in flight time and, consequently, SOC. As can be concluded from Pareto frontiers, such a reduction in climate impact for this scenario is not cheap as only 5% more reduction in climate impact is obtained with almost 4% more increase in SOC (α = 0.0). As the aCCF of contrails is only evaluated in areas favorable for the formation of persistent contrails, typically determined using two inequality constraints, it has sharp spatial behaviors (i.e., PCFA (latitude, longitude, altitude, time) ∈ {0, 1}. In addition, contrails have dominant climate impacts. Therefore, the optimizer's first choice is to avoid forming persistent contrails, which may be achieved more efficiently than reducing the impacts of other species with relatively lower climate impact and smooth spatial behavior. This can be validated in as the lowest priority is given to reducing the climate impact associated with NO_x emission (for $\alpha = 0$).

EUROPEAN PARTNERSHIP

Co-funded by the European Union

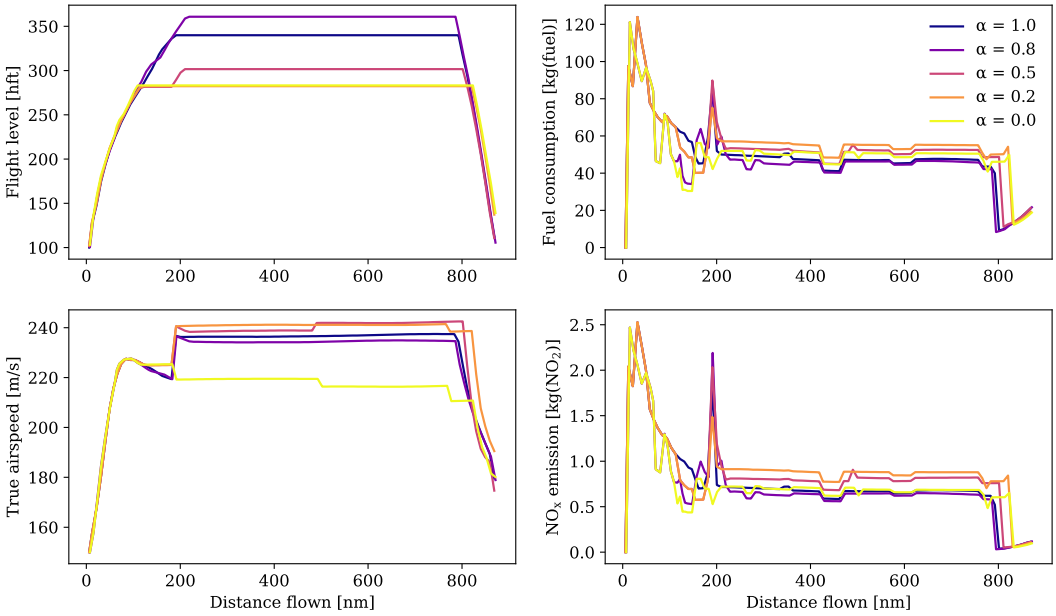

Figure 10. Flight level, fuel burn, true airspeed, and NO_x emission for Case 1 (13th of June 2018, 0000UTC) for different routing options (i.e., α's).

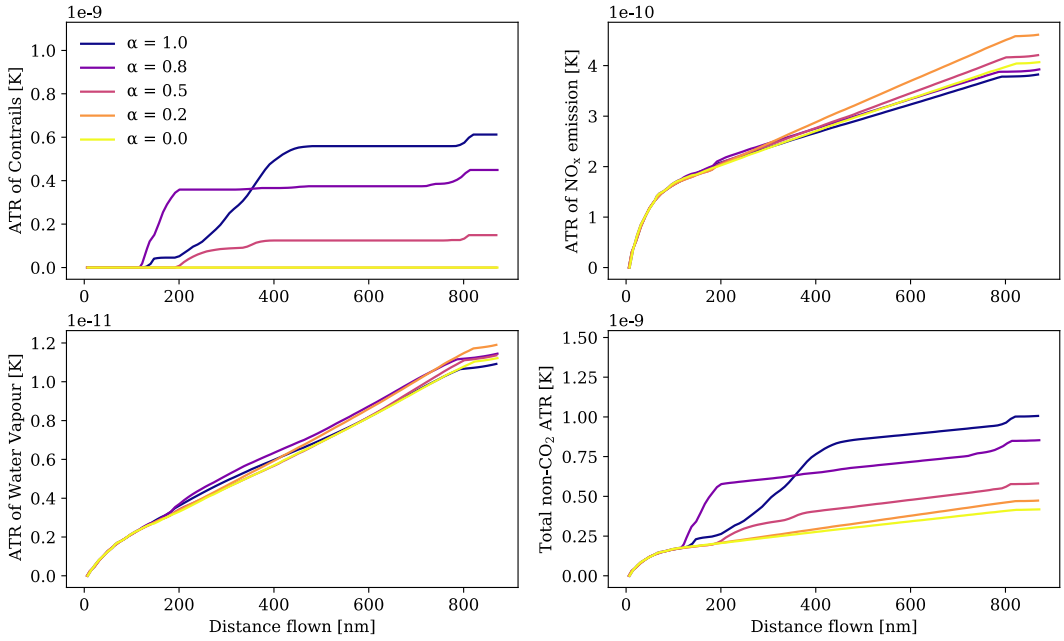

Figure 11. ATRs associated with contrails, NO_X emission, water vapor emission, and total non-CO_2 climate effects (accumulated values along the route) for Case 1 (13th of June 2018, 0000UTC) for different routing options (i.e., α's). The shaded regions show the ranges of uncertainty associated with uncertain meteorological conditions characterized using EPS (outer lighter areas show the minimum and maximum values while the inner darker ones represent 95% confidence interval.

EUROPEAN PARTNERSHIP
Co-funded by the European Union

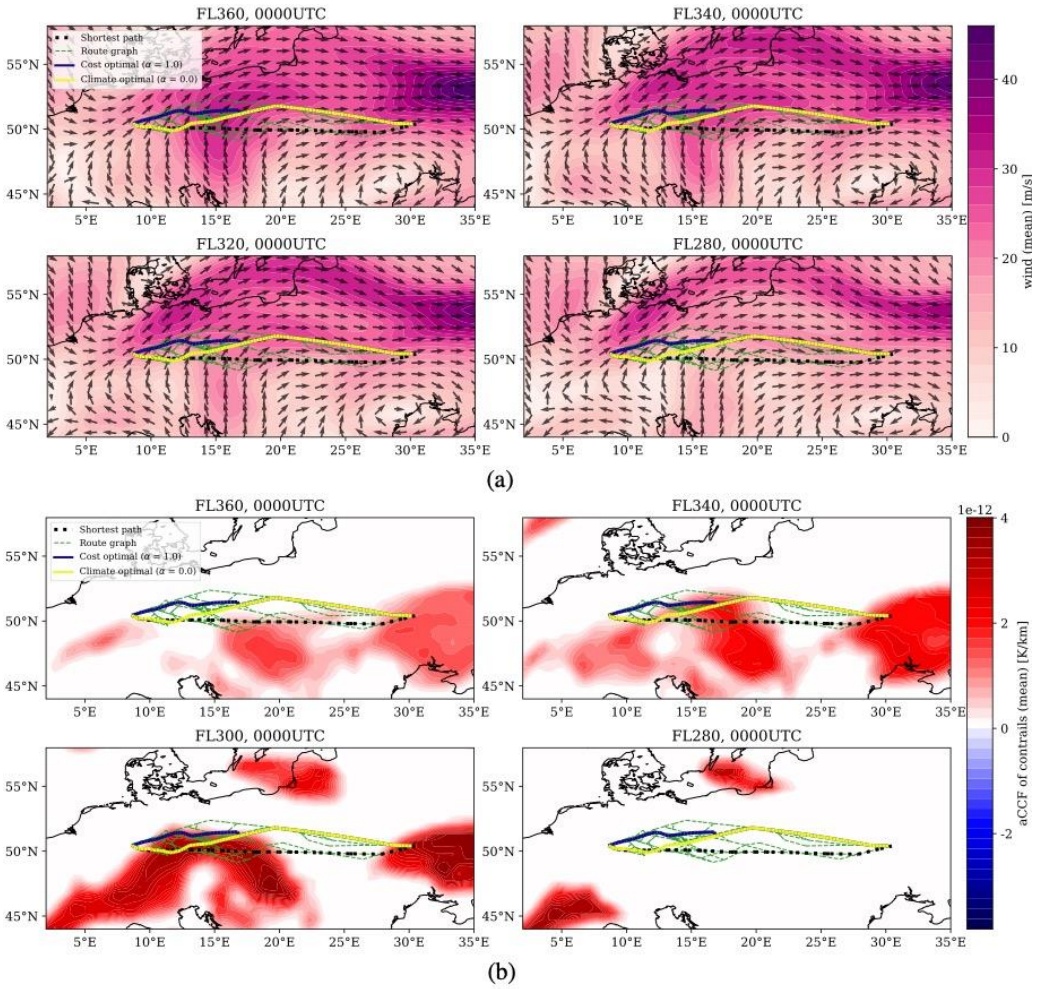

Figure 12. Lateral paths for Case 1 (13th of June 2018, 0000UTC) depicted with (a): wind, (b) aCCF of contrails as colormaps.

EUROPEAN PARTNERSHIP
Co-funded by the European Union

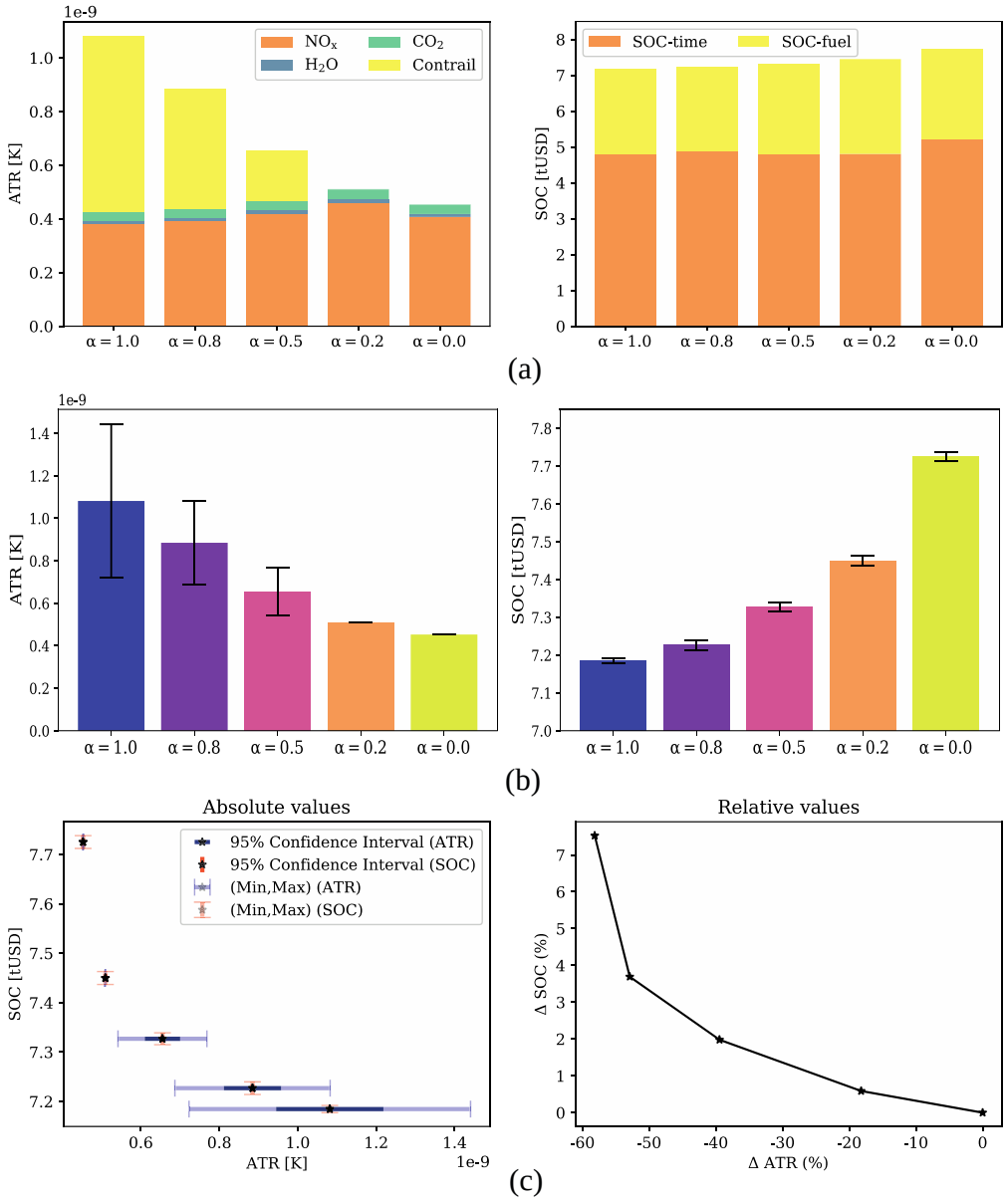

Figure 13. Overall performance of the optimized trajectories in terms of ATR and SOC for Case 1 (13th of June 2018, 0000UTC). (a) Contribution of each species to the total ATR, and costs of flight time and fuel consumption to net SOC (mean values), (b) ATR and SOC with ranges of uncertainty (min-max) for different routing options. (c) Pareto-frontiers considering absolute values (with uncertainty ranges) and relative values (only mean).

3.1.2.2 Example 2 (No formation of persistent contrails)

In the next scenario, we analyze the mitigation potential when no persistent contrails are formed with the cost optimal routing option.

For this case, aircraft profiles and climate responses are depicted in and , respectively. As can be seen in , the optimizer chooses to fly at lower altitudes for routing strategies with higher penalization on

EUROPEAN PARTNERSHIP
Co-funded by the European Union

climate impact. As no contrails are formed (see a), the lateral paths are depicted with the merged aCCF (calculated using mean values of the obtained NO_x emission index) as colormap at different flight levels in b. As can be seen, **flying at lower altitudes is more beneficial in reducing the climate impact of other species (mainly NO_x).** In addition to lowering cruise altitude, the aircraft flies at lower speeds to reduce the fuel flow, and consequently, fuel burnt, NO_x emission index, and NO_x emission. The variability of climate impact and SOC for different α's and Pareto frontiers are given in . By reducing α, the climate impact decreases at the cost of an increase in SOC. For instance, for $\alpha = 0.2$, by accepting a 0.8% increase in cost, a 15% reduction in ATR can be achieved. As in the previous case, the relative increase in SOC is considerable for α = 0, in which the aircraft tends to fly at a relatively lower speed for more reduction in climate impact. In conclusion, climate impact reduction is achieved at the expense of a higher cost increase than in the previous scenario. Moreover, since no contrails are formed, the uncertainty in climate impact is almost neglectable.

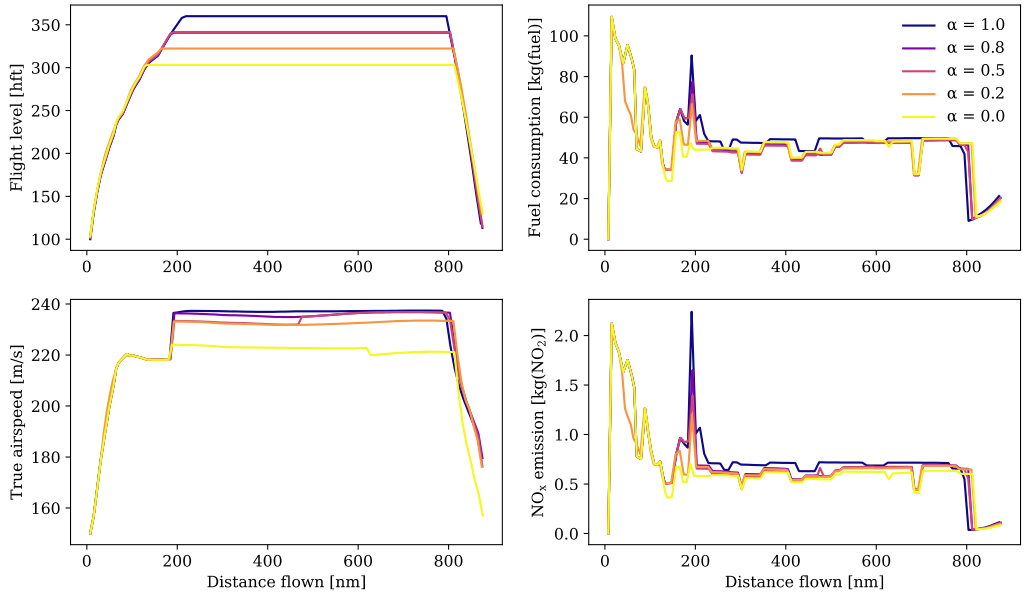

Figure 14. Flight level, Fuel burnt, true airspeed, and NOx emission for Case 2 (10th of December 2018, 1200UTC) for different routing options (i.e., α's).

EUROPEAN PARTNERSHIP
Co-funded by the European Union

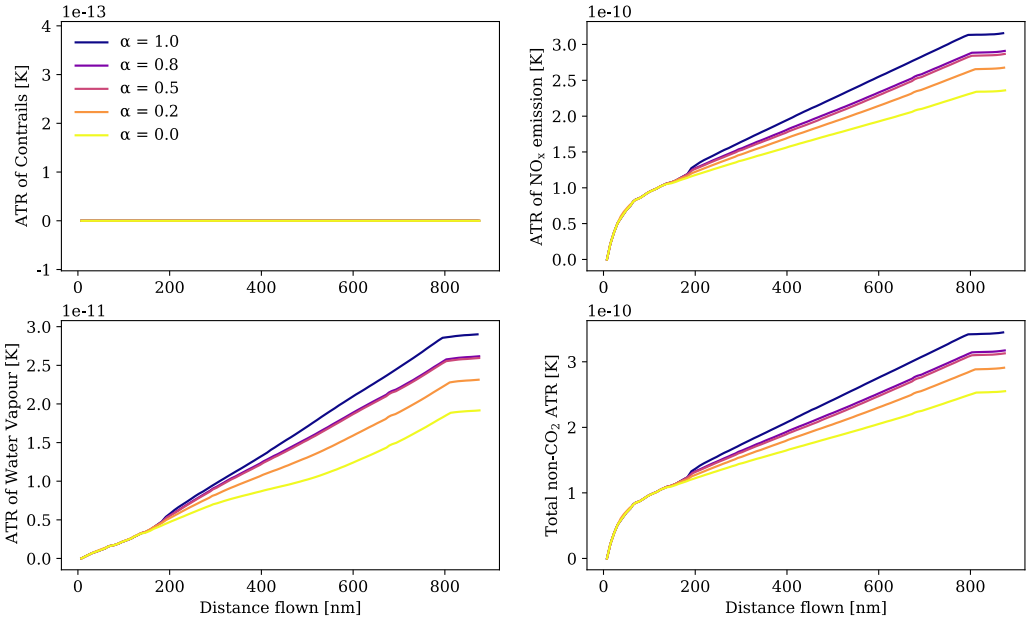

Figure 15. ATRs associated with contrails, NOx emission, water vapor emission, and total non-CO2 climate effects (accumulated values along the route) for Case 2 (10th of December 2018, 1200UTC) for different routing options (i.e., α's).

EUROPEAN PARTNERSHIP
Co-funded by the European Union

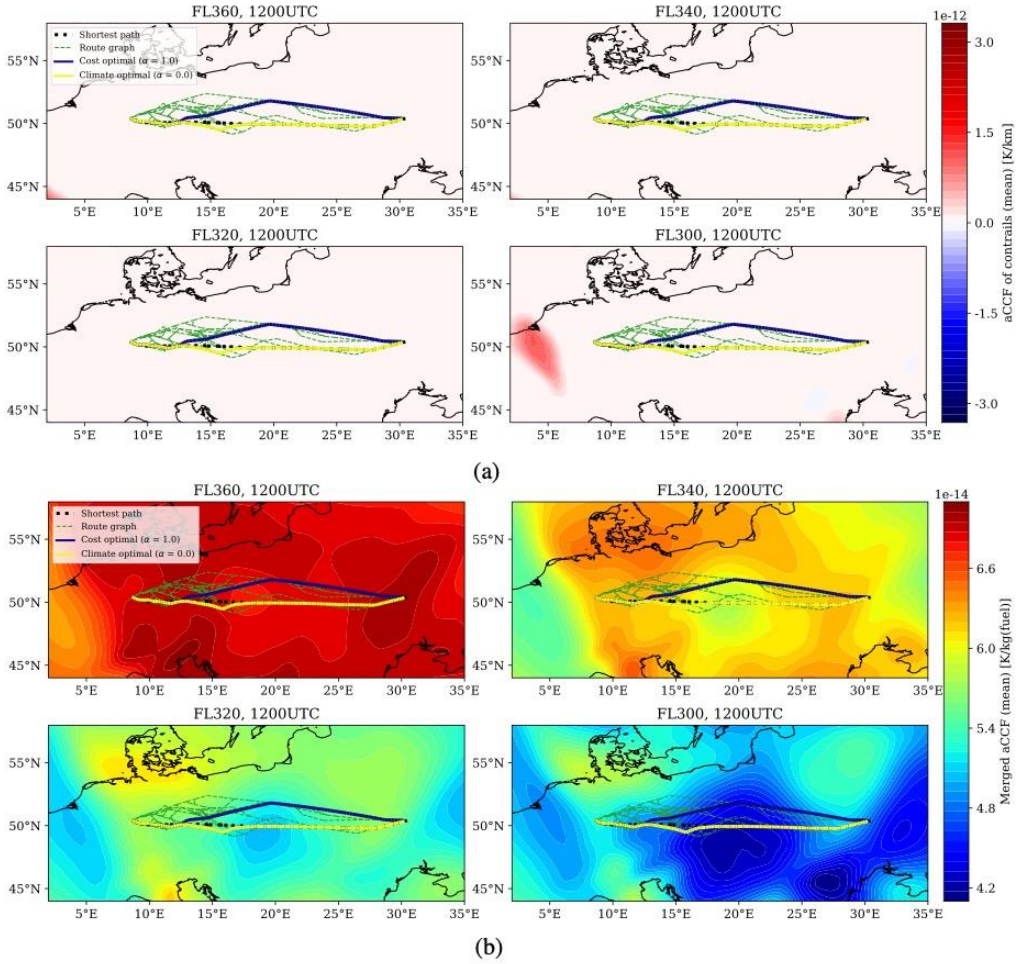

Figure 16. Lateral paths for Case 2 (10th of December 2018, 1200UTC) depicted with (a): aCCF of contrails, (b) merged aCCF.

EUROPEAN PARTNERSHIP
Co-funded by the European Union

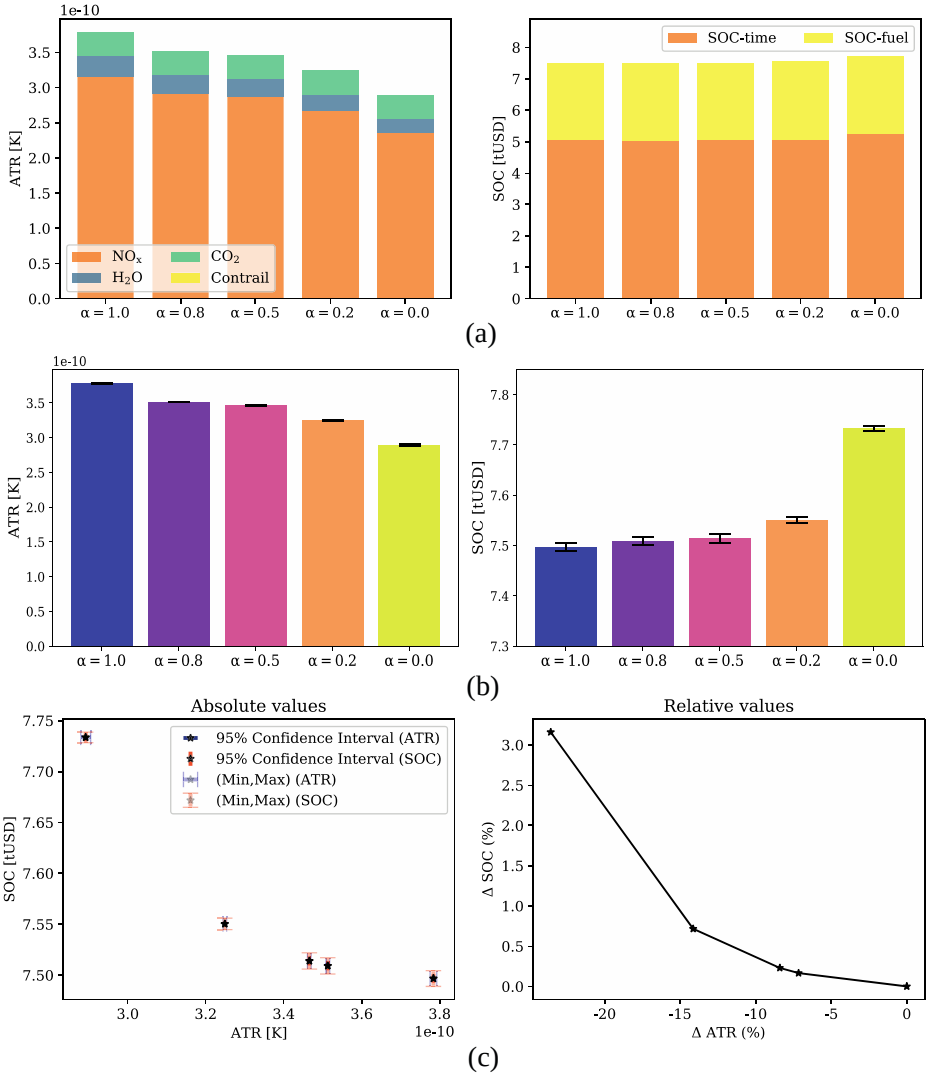

Figure 17. Overall performance of the optimized trajectories in terms of ATR and SOC for Case 2 (10th of December 2018, 1200UTC). (a) Contribution of each species to the total ATR, and costs of flight time and fuel consumption to net SOC (mean values), (b) ATR and SOC with ranges of uncertainty (min-max) for different routing options. (c) Pareto-frontiers considering absolute values (with uncertainty ranges) and relative values (only mean).

3.1.2.3 Example 3 (Formation of persistent contrails during daytime)

A scenario with the formation of cooling contrails is considered for the last case. The aircraft profile and received climate impacts along the route are given in and . It can be seen in that by reducing the value of α, the cooling climate impact of contrails increases. To inverstigate this behavior, lateral paths with the aCCF of contrails as colormaps are depicted in . For the pure climate optimal routing option, the aircraft flies at FL300 and deviates from the shortest path to maximize the cooling impact of contrails. Unlike the case with warming contrails, the uncertainty in the climate impact associated with the climate optimal trajectories is considerable. This is due to the fact that to optimizer chooses to benefit from cooling contrails by flying through highly uncertain persistent contrail formation areas (instead of avoiding them).

EUROPEAN PARTNERSHIP
Co-funded by the European Union

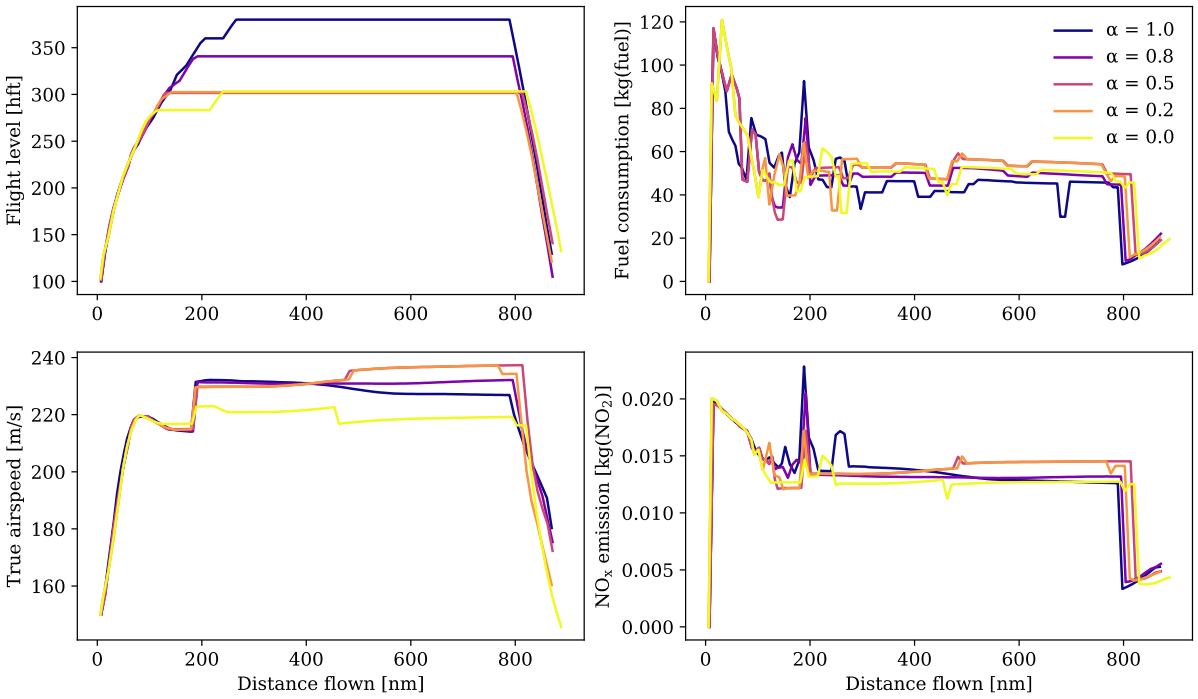

Figure 18. Flight level, Fuel burnt, true airspeed, and NOx emission for Case 1 (10th of December 2018, 1200UTC) for different routing options (i.e., α's).

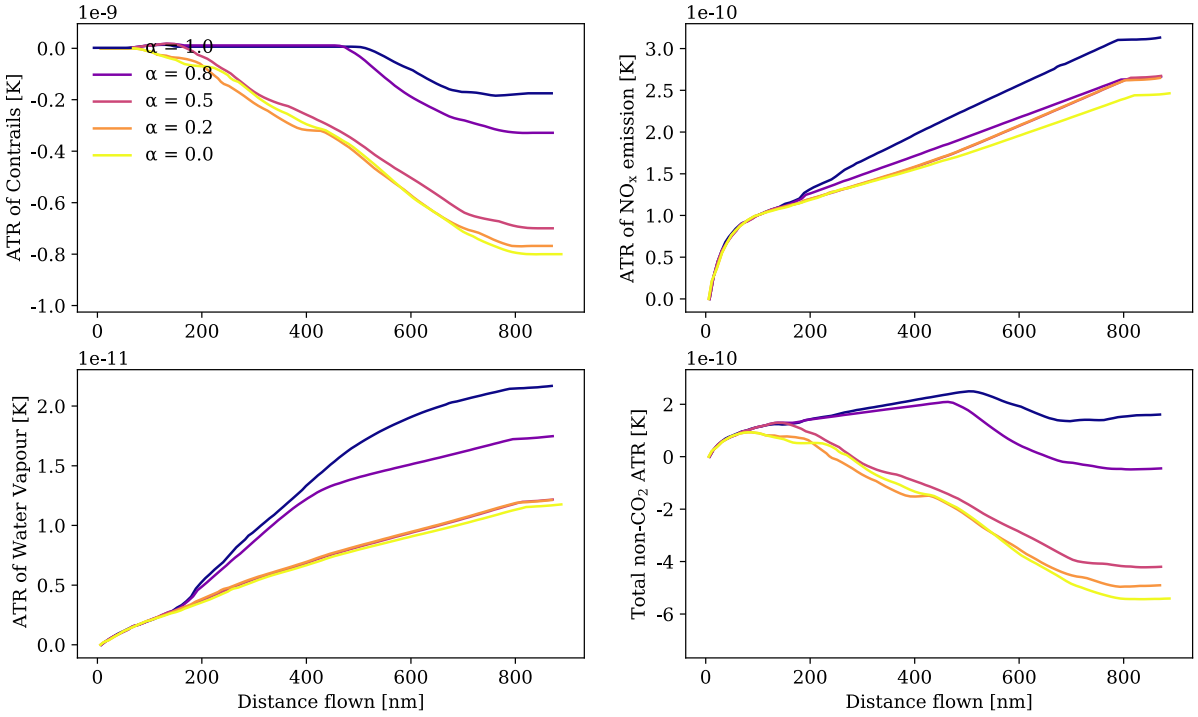

Figure 19. ATRs associated with contrails, NOx emission, water vapor emission, and total non-CO2 climate effects (accumulated values along the route) for Case 3 (20th of December 2018, 1200UTC) for different routing options (i.e., α's).

EUROPEAN PARTNERSHIP
Co-funded by the European Union

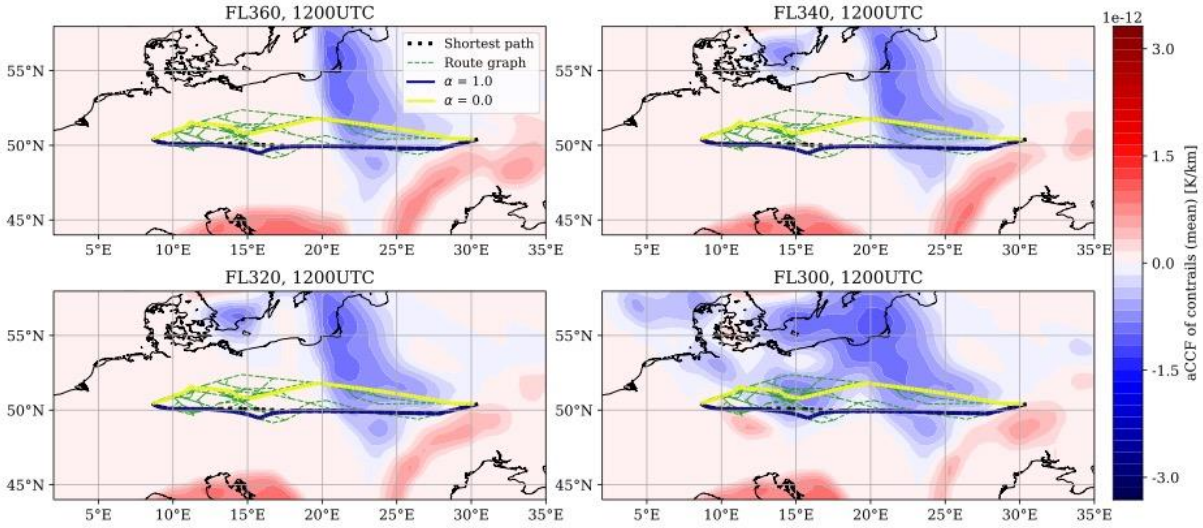

Figure 20. Lateral paths for Case 3 (20th of June 2018, 1200UTC) depicted aCCF of contrails as colormaps.

The contribution of each species to the net climate effect and Pareto-frontiers are provided in . In addition to the increase of contrails' cooling climate impact, warming impacts of NO_x emission and water vapor are also decreased (it can also be verified in). However, when there is not any potential to increase the cooling impact of contrails and decrease the warming impact of NO_x emission spatially through aCCFs, the optimizer tends to fly at a relatively lower speed to decrease NO_x emission in order to reduce the climate impact of NO_x emission (compare the cases $\alpha = 0.0$ and $\alpha = 0.2$ in , in which both fly almost at similar flight levels but different speed). As was shown and concluded in the previous two cases, reducing speed while flying at relatively lower altitudes is not a cheap option to mitigate the climate impact as it increases the flight time and, consequently, SOC. This is also true for this case study (see a). For instance, by looking at the Pareto-frontiers provided in c, we can conclude that a -350% reduction in climate impact can be obtained at the cost of a 3% increase in SOC ($\alpha = 0.2$). However, 25% more reduction is climate impact requires more than 4% additional cost ($\alpha = 0.0$).

EUROPEAN PARTNERSHIP
Co-funded by the European Union

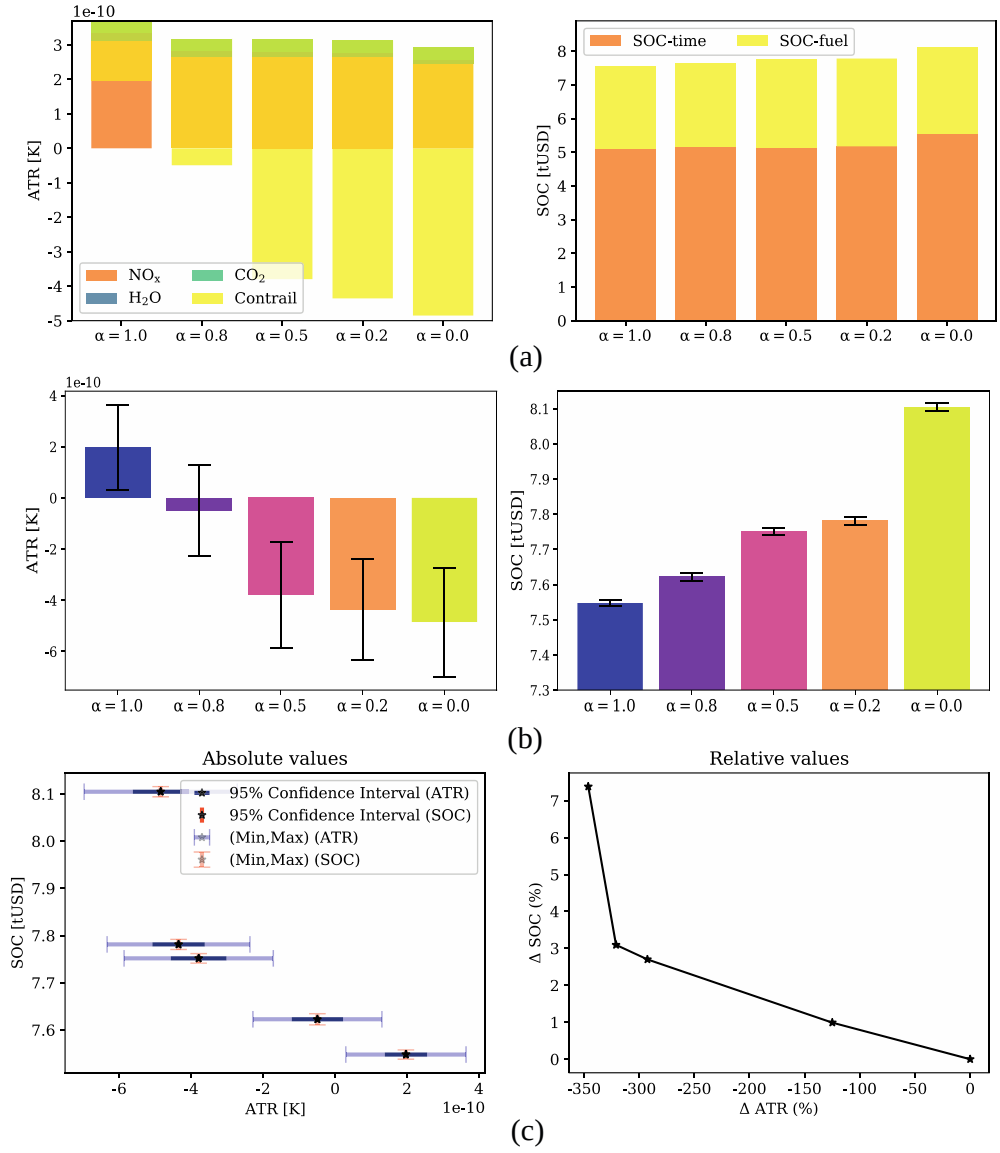

Figure 21. Overall performance of the optimized trajectories in terms of ATR and SOC for Case 3 (20th of December 2018, 1200UTC): (a) Contribution of each species to the total ATR, and costs of flight time and fuel consumption to net SOC (mean values), (b) ATR and SOC with ranges of uncertainty (min-max) for different routing options. (c) Pareto-frontiers considering absolute values (with uncertainty ranges) and relative values (only mean).

Summary

- For a flight from Frankfort to Kyiv on three different days, the mitigation potentials were different due to the change in meteorological conditions.
- The mitigation potentials for scenarios with contrails effects (warming or cooling) were higher due to dominant climate impact and non-smooth spatial behavior of contrails. In such cases, the optimizer's first choice was to reduce the warming impact or increase the cooling impact of contrails.

EUROPEAN PARTNERSHIP
Co-funded by the European Union

- The climate effects of contrails were highly uncertain. The relatively high uncertainty in contrails' climate impact is related to the high variability among the ensemble members of relative humidity provided by the EPS required to determine the areas favorable for forming persistent contrails.

- The generation of cooling contrails was associated with high uncertainty as the aircraft tends to fly within uncertain persistent contrail formation areas. However, the results were received almost deterministic for the scenarios with no contrails or the cases where aircraft trajectories avoid the formation of contrails.

3.1.3 Mitigation potential

This section includes general conclusions drawn from individual and representative case studies applied to the traffic scenario considered within WP2. Results, as well as uncertainties are presented in a consolidated manner for the top 100 routes and selected days.

3.1.3.1 Daily and Seasonal impacts

In this section, results will be presented to highlight the daily and seasonal variability and impact of atmospheric conditions on the optimized trajectories. The variability of the contrails climate impact quantified employing aCCF of contrails over the selected days in June and December is depicted in on pressure levels 200, 250, 300, and 350hPa for 0000UTC and 1200UTC. Notice that the aCCF of contrails is considered as colormaps due to its dominant climate impact, playing an important role in determining aircraft trajectory in a climate-friendly manner. As can be seen, at midnight (i.e., 0000UTC), the contrails climate impact is warming, while at midday, in addition to warming impacts, there are some areas with cooling climate effects. Besides, strong daily and seasonal variability can be concluded.

The results of optimizing the top 100 routes for the considered scenarios is depicted in . Notice that results are presented per flight using weights associated with ASK of routes for averaging. For each day, three columns are given, respectively, showing the best climate impact mitigation potentials allowing +0% (cost-optimal), 1%, and 2.5% increases in the cost (quantified using SOC) corresponding to the cost optimal routing option. As can be seen, by adopting more increases in SOC, we can reduce more climate impacts. The mitigation potentials are strongly variable due to the change in atmospheric conditions. Such variability is higher for the contrails climate impact. Similar to the single route analysis, the focus of the optimizer for the aggregated results is on reducing the warming impact or increasing the cooling impact of contrails. By referring to and looking at the obtained aggregated results, one can conclude that the mitigation potential is higher for those cases with more formation of persistent contrails at altitudes aircraft usually fly within the minimum cost routing strategy. For instance, more persistent contrails are formed on 05th, 10th, and 25th December 2018, 0000UTC for the area covering the top 100 routes than on the 15th and 20th of that month (see pressure levels 200 and 250hPa). Thus, the mitigation potentials for those days are received higher (as was also concluded for single route analysis).

In addition, during the daytime, it is possible to have cooling impacts of contrails for all days in December except for the 10th. This can be verified by referring to , in which no cooling impact is identified by aCCF of contrails during the daytime on the 10th of December for the area covering the top 100 routes. No potentiality to have the cooling impact of contrails in June can also be justified with .

Pareto-frontiers generated considering 0.0%, 0.01%, 0.05%, 0.1%, 0.5%, 1.0%, 1.5%, 2.0%, and 2.5% increases in cost are depicted in Figure 29 for absolute values with uncertainty ranges, mean of relative absolute values, and mean of the normalized relative values in percentage. It can be concluded that the climate impact mitigation potentials vary between 16% to 53%, with a maximum 2.5% increase in SOC of the pure cost optimal scenario. In addition, the ranges of uncertainty in net climate effects for the climate optimal trajectories resulting in the cooling climate impacts of contrails is relatively higher than the cases with only warming impacts in which the optimizer tends to avoid forming persistent contrails. For instance, let us compare the aggregated results, providing the best mitigation potentials in December at 0000UTC and 1200UTC, which are the 25th of December, 0000UTC, and 05th of December, 1200UTC. As can be seen, for nighttime flights, the range of uncertainty reduces because aircraft tend to avoid the formation of warming contrails. In contrast, for daytime flights, aircraft fly through uncertain PCFA regions to increase the cooling impact of contrails.

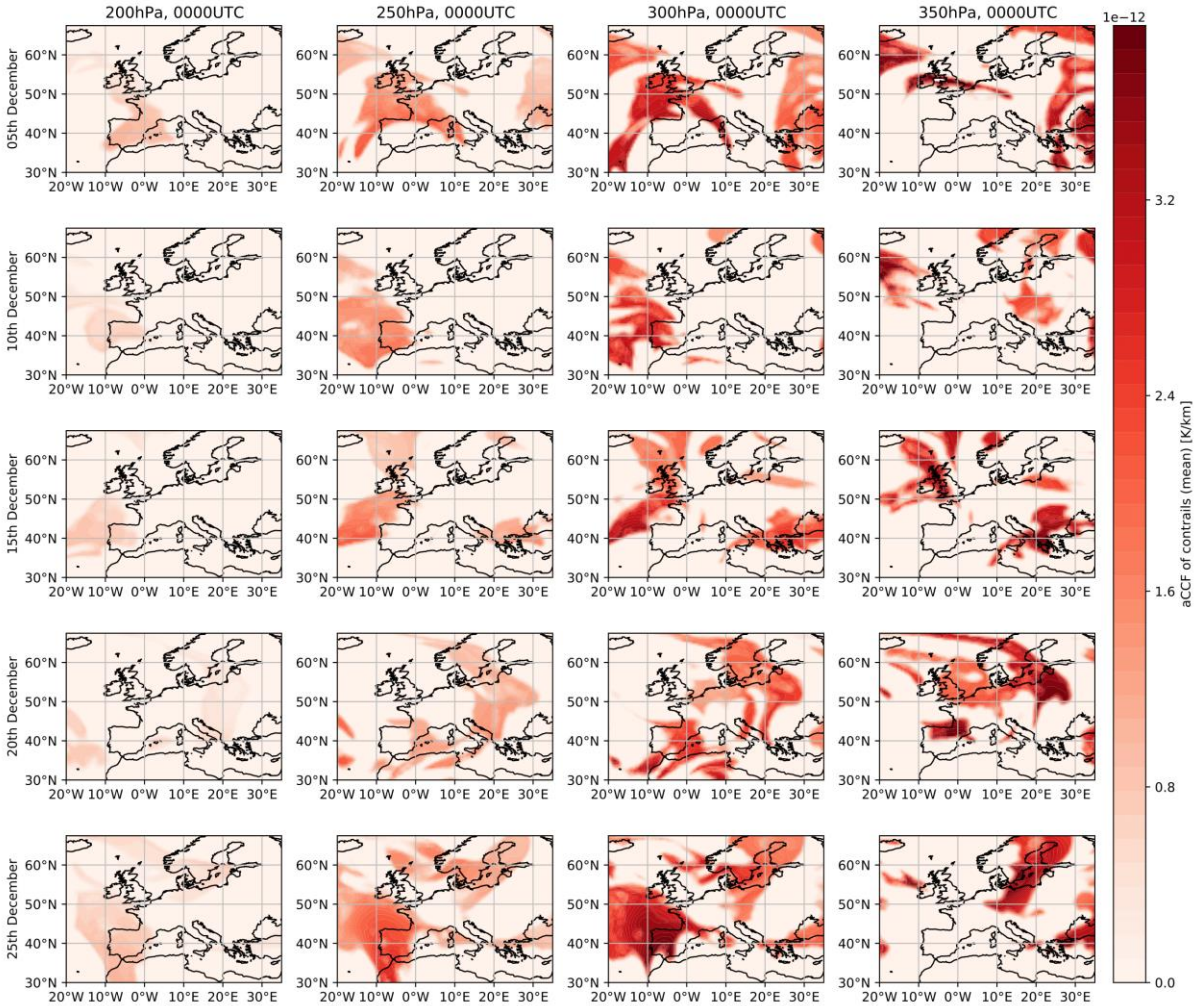

Figure 22. Algorithmic climate change function of contrails for the selected days in December 2018 at 0000UTC for different pressure levels.

EUROPEAN PARTNERSHIP
Co-funded by the European Union

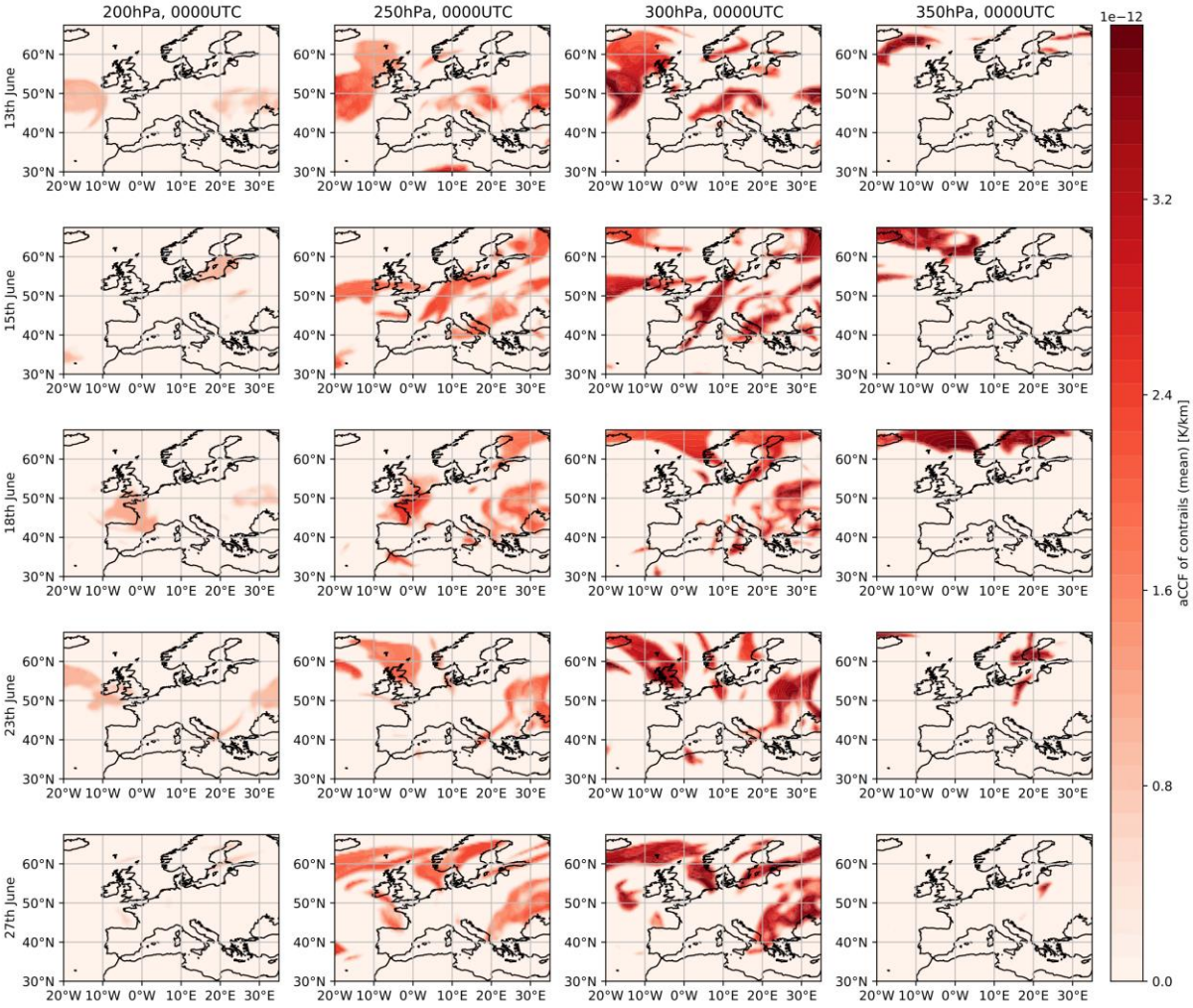

Figure 23. Algorithmic climate change function of contrails for the selected days in June 2018 at 0000UTC for different pressure levels.

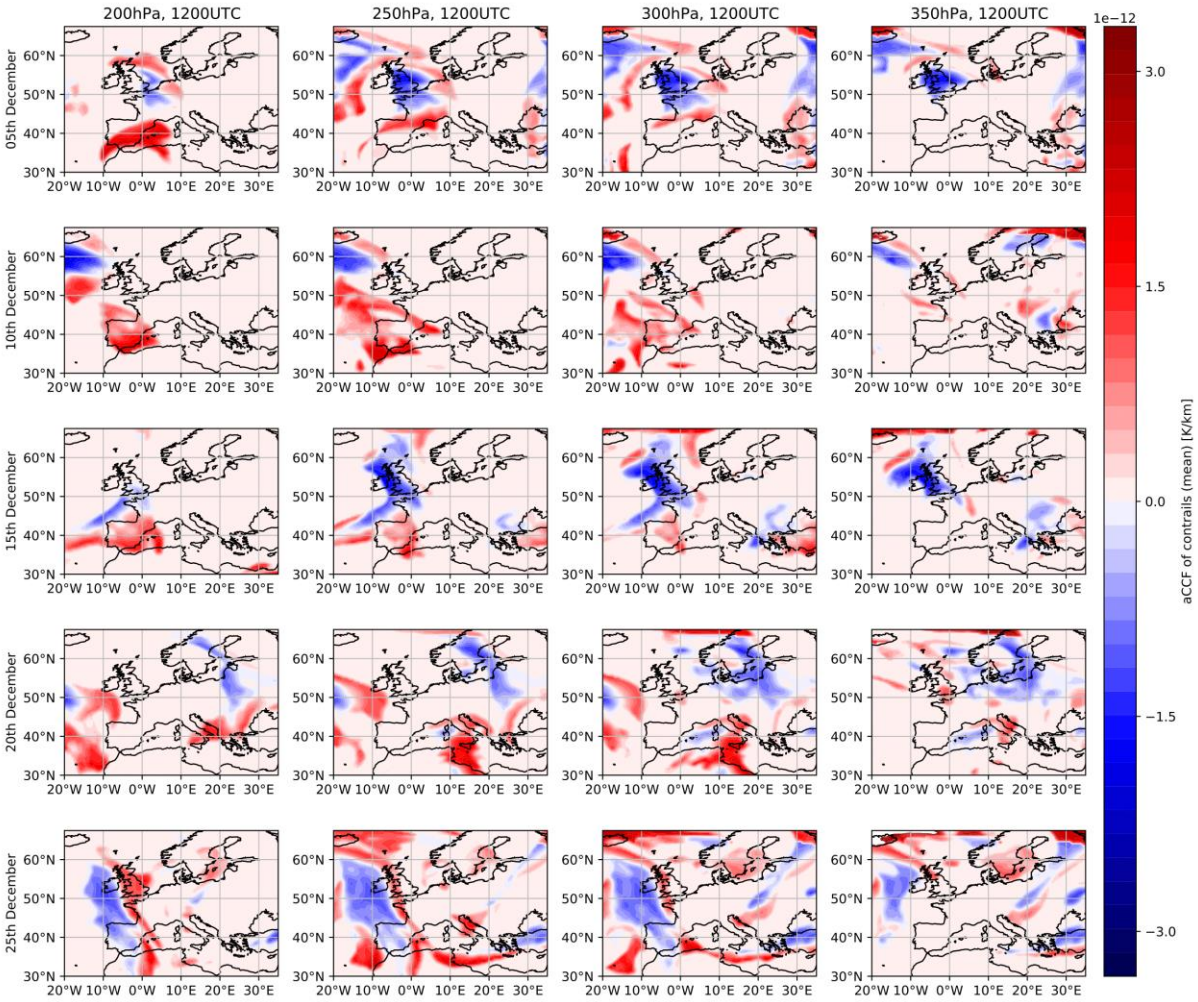

Figure 24. Algorithmic climate change function of contrails for the selected days in December 2018 at 1200UTC for different pressure levels.

EUROPEAN PARTNERSHIP
Co-funded by the European Union

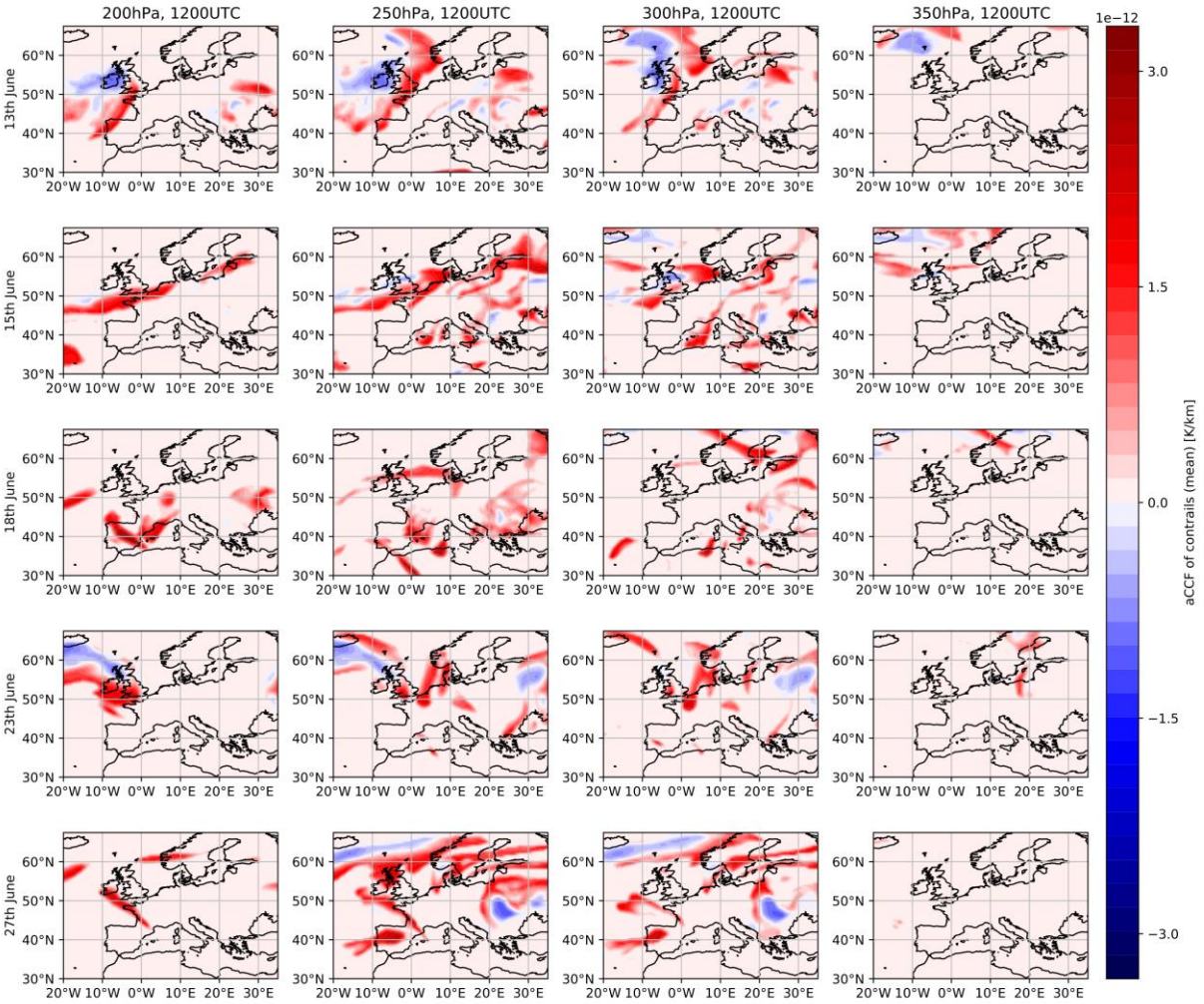

Figure 25. Algorithmic climate change function of contrails for the selected days in June 2018 at 1200UTC for different pressure levels.

EUROPEAN PARTNERSHIP
Co-funded by the European Union

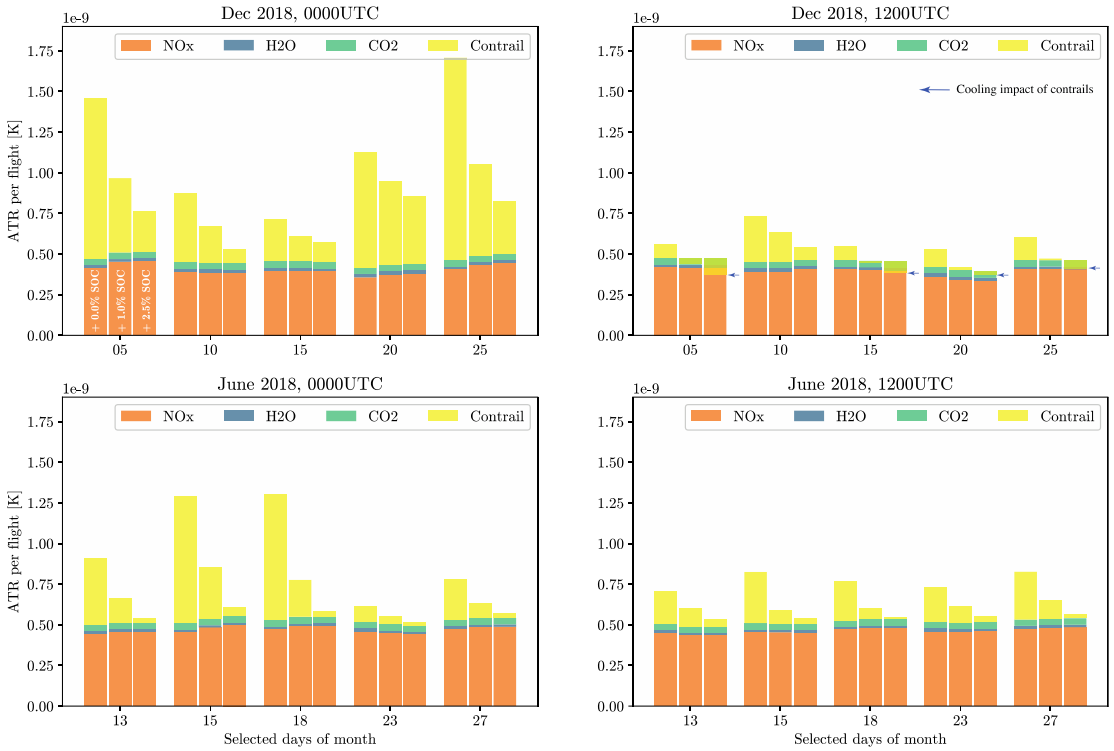

Figure 26. Aggregated results of optimizing the top 100 routes: Contribution of each species to net ATR for the most climate optimal scenario accepting 0.0%, 1.0% and 2.5% increase in SOC.

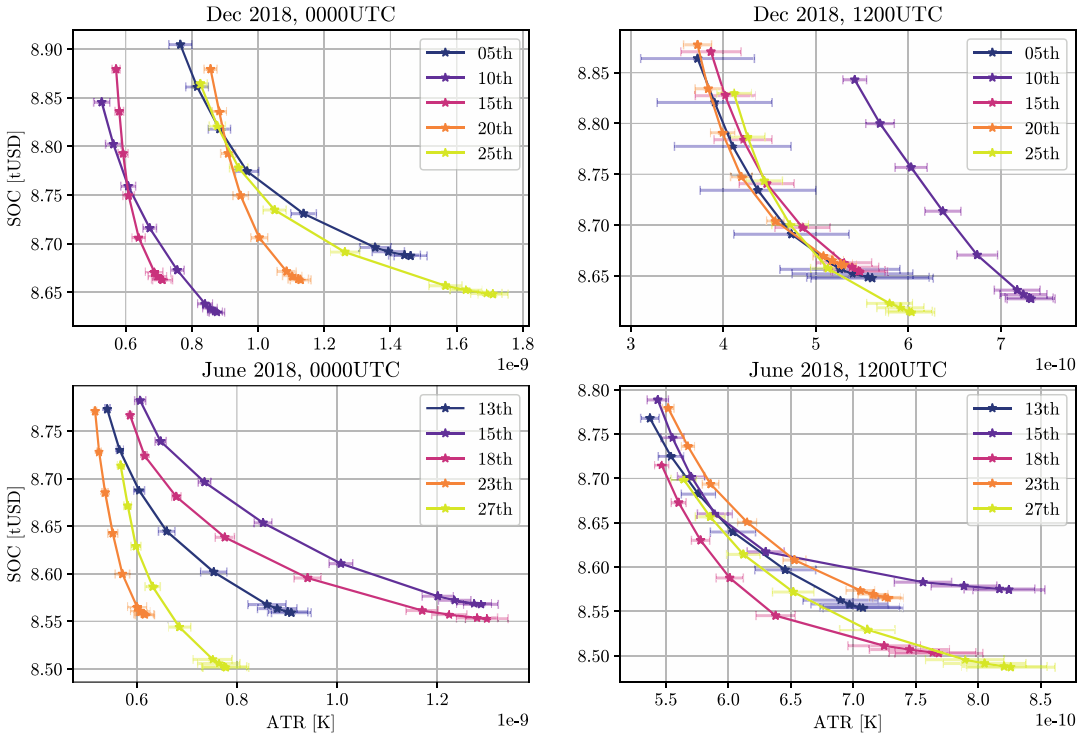

Figure 27. Aggregated results of optimizing the top 100 routes: Trade-off between reducing climate impact and relative increase in SOC considering absolute values.

EUROPEAN PARTNERSHIP
Co-funded by the European Union

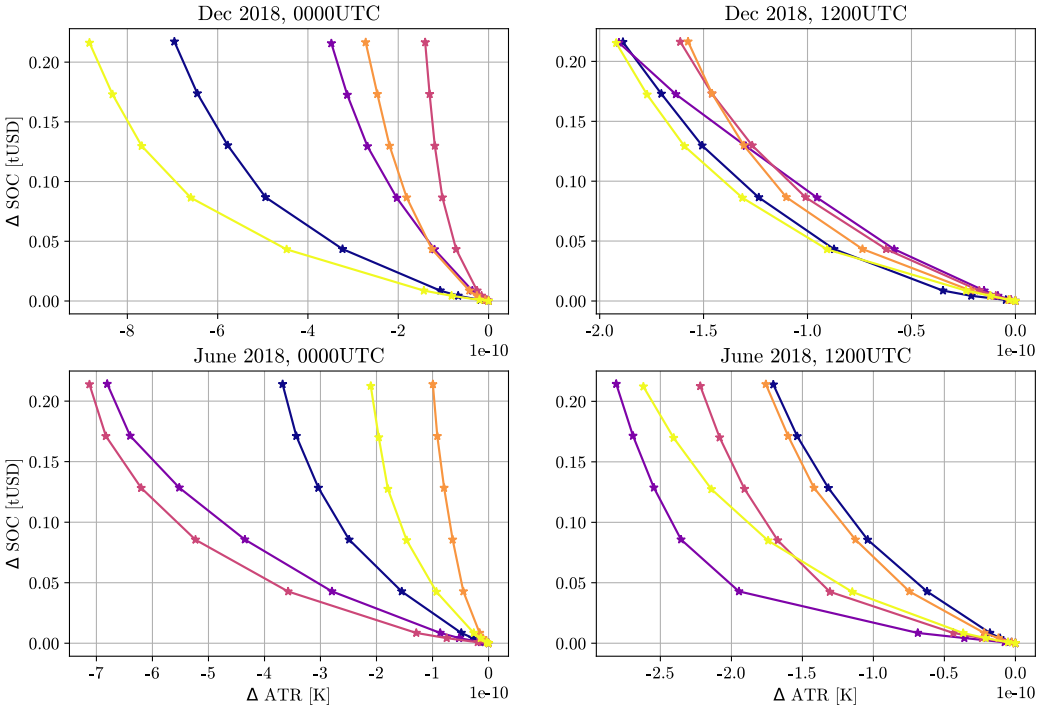

Figure 28. Aggregated results of optimizing the top 100 routes: Trade-off between reducing climate impact and relative increase in SOC considering relative values.

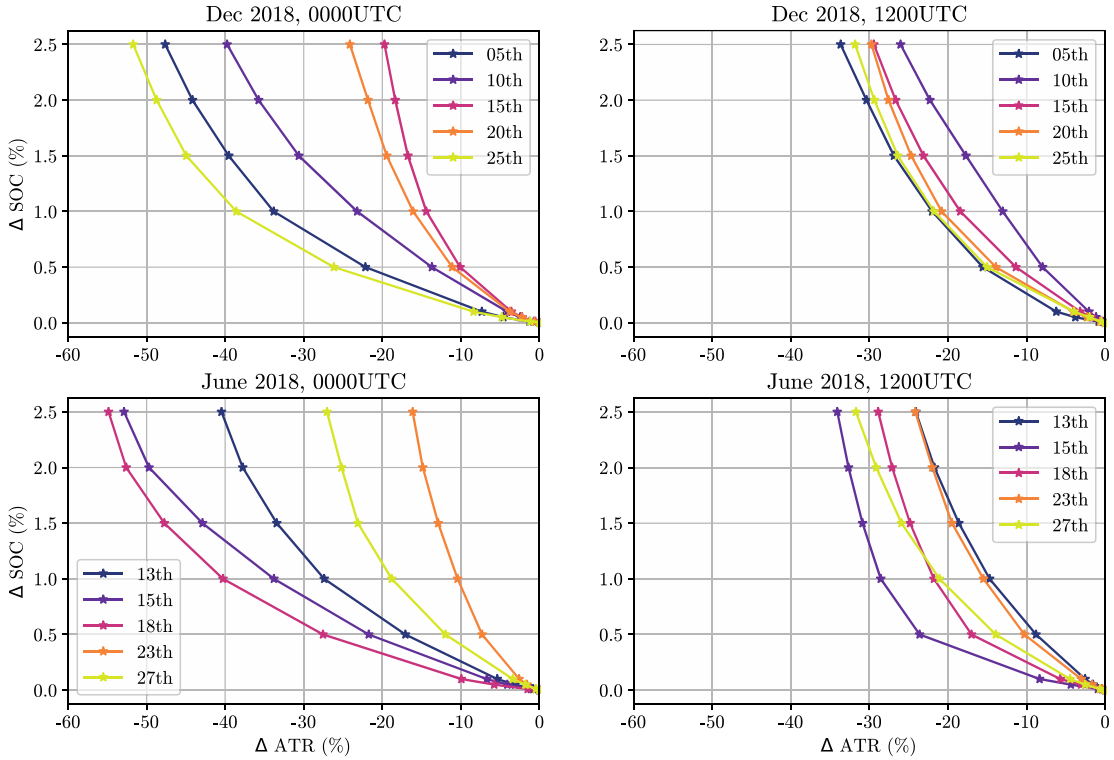

Figure 29. Aggregated results of optimizing the top 100 routes: Trade-off between reducing climate impact and relative increase in SOC considering normalized relative values in percentage.

EUROPEAN PARTNERSHIP
Co-funded by the European Union

Summary

For the aggregated results, a similar behavior to the single route analysis can be concluded:

- The received mitigation potentials were variable due to the change in atmospheric conditions.
- For the considered case studies, in general, the nighttime flights resulted in more reduction of climate impacts (≈ 16-53%) compared to the daytime (≈ 23-34%).
- The mitigation potentials were mainly achieved by reducing the warming impact or increasing the cooling impact of contrails.
- Overall, allowing a maximum 2.5% increase in cost could reduce the climate impact by 16-53%
- The uncertainties on those results generating cooling contrails were high due to the tendency to fly through uncertain persistent contrails formation areas.
-

3.2 Results based on the continuous optimal control approach

The results estimated with TOM as described in section 1.1.1 on the basis of the previously introduced fictitious route network in section 2.1.3 are presented in the following in two sections. The overall mitigation potential is estimated using a three-step procedure: First, a deterministic pareto-front is generated for each route and each ensemble member of the weather forecast. Secondly, for each route, the pareto fronts of all ensemble members are combined in order to obtain probabilistic pareto fronts (see section 3.2.1). Finally, the results are aggregated for the top 10 routes of the ficiticious route network for the summer and the winter period (June and December) and for different times of the day (00:00 UTC and 12:00 UTC) as illustrated in section 3.2.3.

3.2.1 Single Route analysis

Within this section, step 1 and step 2 of the evaluation methodology are explained and exemplary results of optimised trajectories under consideration of uncertainties are presented and discussed. Section 3.2.1.1 highlights the estimation of a pareto front for one emseble member and section 3.2.2 focuses on the determination of a probabilistic pareto-front based on the pareto fronts for each of the ensembles.

3.2.1.1 Pareto front for one ensemble member

Considering both, climate impact and economic aspects in the optimization of trajectories, 50 pareto-optimal trajectories for each of the top 10 routes and each ensemble of the selected weather situations have been calculated by systematically varying the weighting factors c_{clim} and c_{SOC} according to Equations (4) and (5). Here, we optimize the most relevant route in terms of ASK from our fictitious network depicted in Figure 30 for the 13th and 18th of June 2018 at 00:00 UTC. As illustrated in Figure 30, the minimum cost trajectory (black, c_{SOC} = 1) shows a shift eastwards when compared to the orthodrome (blue) in order to benefit from the reduced headwinds over the Bay of Biscay between Spain and France. **Since we are considering night-time conditions, contrails have exclusively warming effects as opposed to day-time contrails** as can be observed on the exclusively red contrail areas (red – warming effect, blue – cooling effect). The considered route is unaffected by contrails on June 13th

EUROPEAN PARTNERSHIP

Co-funded by the European Union

(see Figure 30 and Figure 32) but goes through a strong contrail formation area on June 18th (see Figure 33 and Figure 35).

Example 1: Spanish Riviera (CG) – London (FG), 2018-06-13 00:00 UTC (no contrail impact)

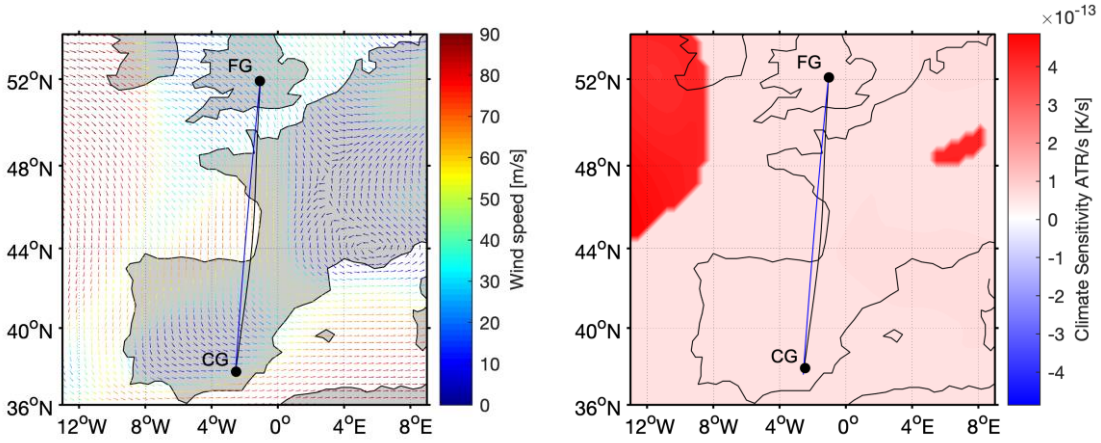

Figure 30. Optimized trajectories for the fictitious route with highest ASK volume on the 13th of June 2018 00:00 UTC departing from southern Spain and destined towards the greater London area.

In Figure 30 the lateral path of the minimum SOC trajectory (black) and orthodrome (blue) are illustrated including the wind situation (left) and the total climate sensitivity (right) at an average altitude of 11.091 m. The lateral path of the minimum climate impact trajectory is not shown separately, since it only deviates slightly from the minimum cost trajectory. We can observe a field of head winds across the middle section of the route, and no contrail-sensitive areas on cruise altitude. This lack of contrail-senstitive regions influences the pareto front as the next highest impact is caused by ozone. This can also be observed in Figure 31, where the shape of the pareto-front is clearly dominated by ozone and on a smaller scale water vapor.

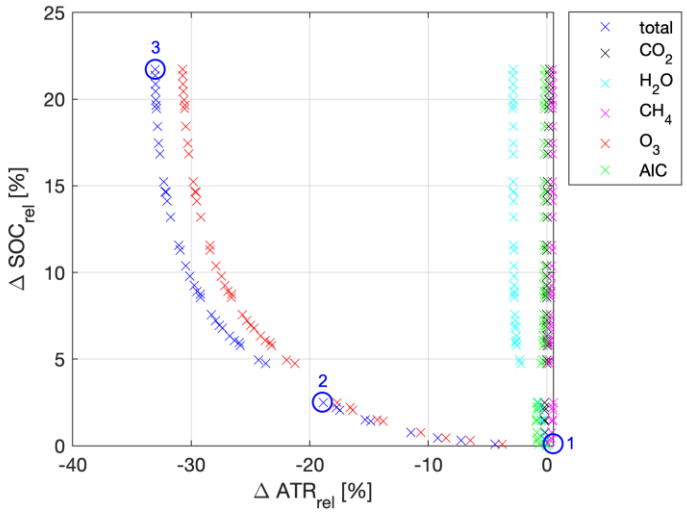

Figure 31. Pareto front for the 13th of June 2018 0000 UTC. 50 different parameter combinations were applied to generate the pareto front.

EUROPEAN PARTNERSHIP
Co-funded by the European Union

The parameter sweep performed to generate the pareto-front ranges from fuel optimal to climate optimal routes. A total relative climate impact mitigation potential of 33% can be achieved when comparing to a reference trajectory optimized for cost. This potential is dominated by the ozone aCCF, which allows for mitigation by deviating the trajectory to lower cruise altitudes. Due to the absence of contrail-forming regions the contrail aCCFs does not contribute any mitigation potential.

From the 50 different parameter combinations optimized we present three characteristic points as depicted in Figure 31. Ranging from the cost optimal Point 1, we achieve a relative mitigation potential of about 19% for a relative increase in cost of 2,5%. Further decreasing the penalty of cost in the optimization leads to the maximum possible relative climate impact mitigation under the given boundary conditions of 33% at a relative increase in SOC (which considers both fuel and time).

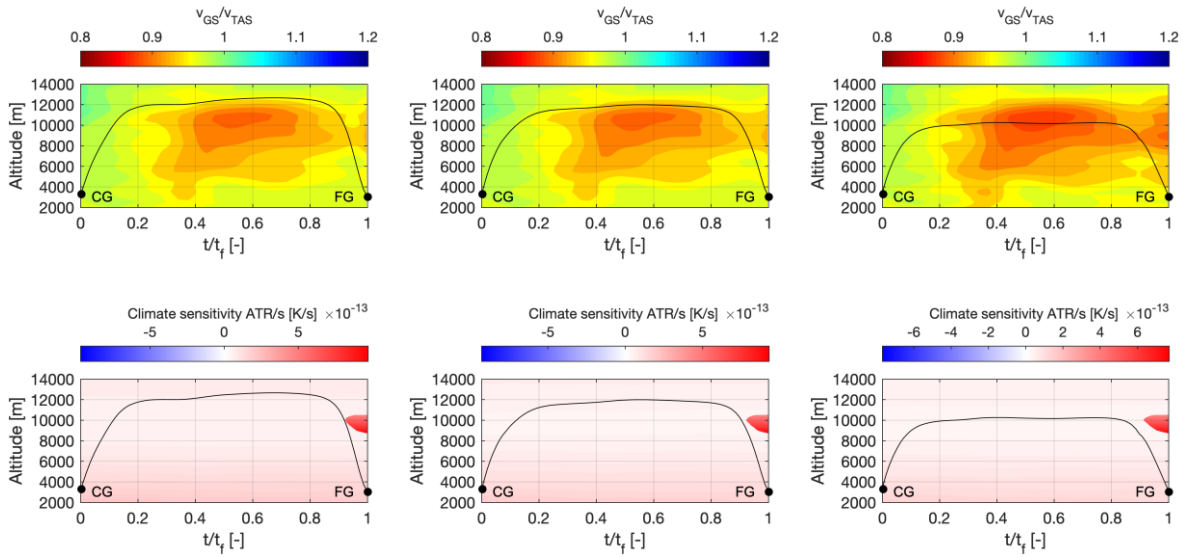

Figure 32. Altitude profiles of wind and contrail-aCCF for the 13th of June 2018. The lateral paths are shown for the minimum climate impact case (right, Point 3 of pareto-front), the minimum cost case (left, Point 1 of pareto-front) and an intermediate step (Point 2 of pareto-front) as a function of the relative flight time t/t_f.

The wind situation for the vertical trajectories is indicated as a ratio between ground speed v_{GS} and true airspeed v_{TAS}. Values greater than one indicate tailwind areas, values smaller than one indicate headwind areas. When considering the climate optimal case, we can observe a lower cruise altitude flown to minimize climate sensitive regions present in higher flight levels. This however causes the route to cross directly through a field of headwind, thus prolonging the flight time and increasing total fuel burn and hence costs. The cost optimal case ascends into a higher altitude at about t/tf = 0.4 and avoids a headwind area which is present at lower altitudes.

Example 2: Spanish Riviera (CG) – London (FG), 2018-06-18 00:00 UTC (large contrail impact)

The second investigated day for the trajectory CG-FG is the 18th of June. This day was selected due to the strongly different atmospheric conditions, and thus different optimized routes.

EUROPEAN PARTNERSHIP
Co-funded by the European Union

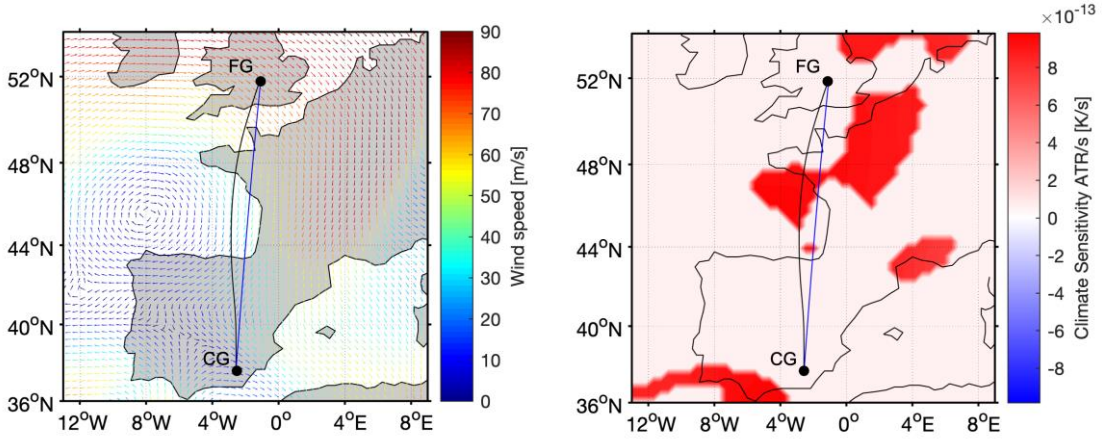

Figure 33. Optimized trajectories for the fictitious route with highest ASK volume on the 18th of June 2018 0000 UTC.

The lateral path of the minimum fuel trajectory (black) and orthodrome (blue) are illustrated including the wind situation (left) and the total climate sensitivity (right) at an average altitude of 10,819 m. The lateral path of the minimum climate impact trajectory is not shown separately, since it only deviates slightly from the minimum cost trajectory. Compared to the previous example route without any contrail sensitive regions, here a clear lateral and vertical deviation can be observed. The lateral deviation is mainly caused by taking advantage of tailwinds causing a westward shift at latitudes between 42°N and 51°N. Since **the lateral expansion of contrails is generally higher than the vertical one, the optimizer avoids contrail-sensitive regions by changing the vertical profile** of the trajectory. This smaller deviation consequently causes a lower cost increase when compared to a lateral avoidance. Furthermore, the prevailing headwinds also have an impact on the vertical profile, causing a dip from about 11,000m at t/tf = 0.2 and an ascend back to almost 12,000m to decrease flight time in regions with headwind.

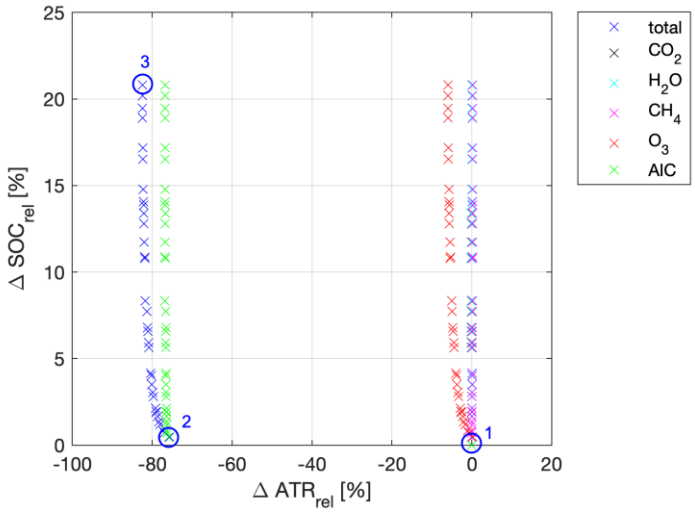

Figure 34. Pareto front for the 18th of June 2018 00:00 UTC. 50 different parameter combinations were applied to generate the pareto front.

EUROPEAN PARTNERSHIP
Co-funded by the European Union

The parameter sweep for the pareto front shown in Figure 34 ranges from cost optimal to climate optimal routes. The presence of contrails is the main contributor the shape and total mitigation potential observed in the pareto front. **Since avoiding the contrail-sensitive region vertically has little economical consequences, a large reduction in relative ATR can be achieved at minimal cost increase** as highlighted by Point 2 in Figure 34. A total relative climate impact mitigation potential of 82% can be achieved when comparing to a reference trajectory optimized for minimal costs (Point 3).

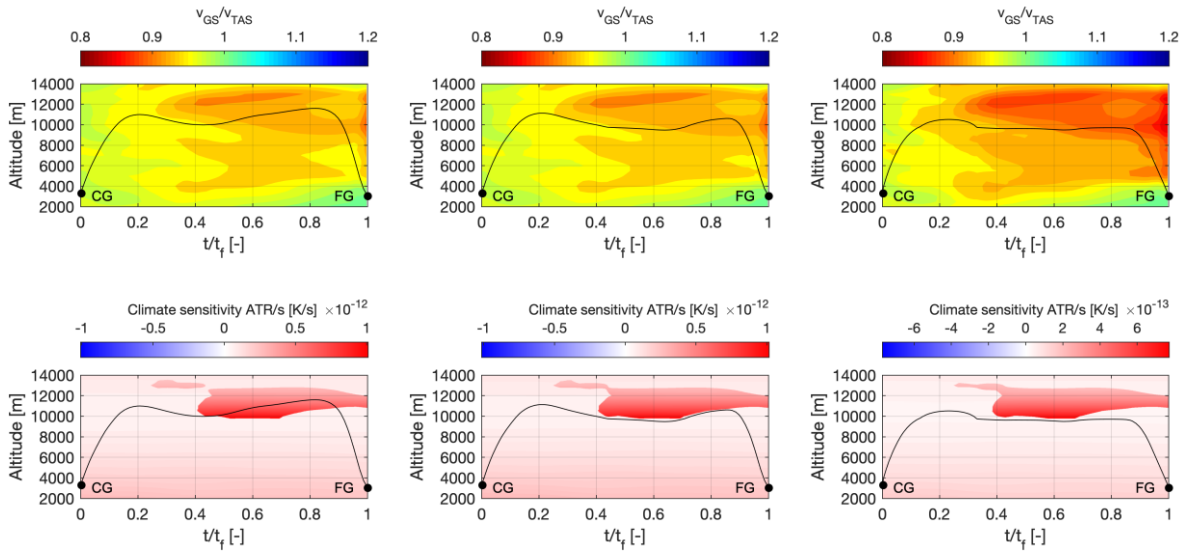

Figure 35. Altitude profiles of wind and contrail-aCCF for the 18th of June 2018. The lateral paths are shown for the minimum climate impact case (right), and the minimum fuel case (left) as a function of the relative flight time t/t_f.

Again, here the wind situation for the vertical trajectories is indicated as a ratio between ground speed vGS and true airspeed vTAS. Values greater than one indicate tailwind areas, values smaller than one indicate headwind areas. When observing the climate optimal case (right), a dive starting at t/tf = 0.3 is visible which is caused by both the field of headwind and the contrail-sensitive area ahead. The cost optimal case ascends into a higher altitude at about t/tf = 0.4 and minimizes flight time crossing areas of headwind.

3.2.2 Probabilistic pareto front

Taking into consideration the same route as previously presented, in this section we include results for the optimization of the trajectory for the set of ten ensembles to include the uncertainty related to weather variability. Individual pareto fronts are combined for all ensembles, e.g., see Figure 36 (b). Minimun and maximum values are determined for all 50 parameter combinations and the mean value is calculated Figure 36(c). Finally, the contributions of individual emission species are are estimated for the whole set of trajectories as seen in Figure 36 (d).

EUROPEAN PARTNERSHIP
Co-funded by the European Union

Example 1: Spanish Riviera (CG) – London (FG), 2018-06-13 0000 UTC (no contrail impact)

The previously shown results for the single route example where computed on the basis of a single ensemble member of the EPS forecast. Here, we further analyze the influence of the whole set of ten ensembles to assess the impact of uncertainty in the weather prediction on the solutions generated with TOM. For this we have optimized the same route individually for each of the ensemble members, which renders ten different pareto-fronts. We determine maxima, minima and mean values for each parameter combination with shifting weights on climate and cost penalty. Finally, the mean impact of individual emission species is analyzed per route.

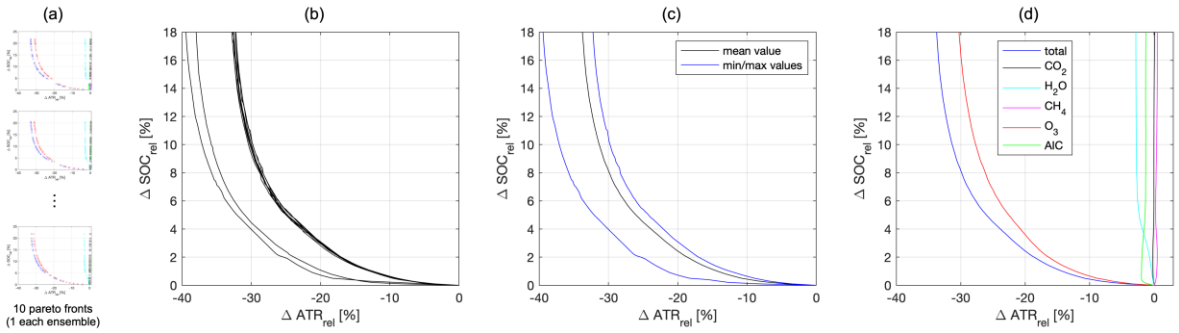

Figure 36. Probabilistic Pareto-fronts for the most relevant fictitious route. Individual Pareto-fronts (a) are aggregated (b) to evaluate minima, maxima and mean values for each optimization step (c). Finally, contributions of individual emission species (d) are determined for the trajectory and ten weather scenarios of the 13th of June 2018.

Individual Pareot-Fronts, see Figure 36(a) are aggregated (b) to evaluate minima, maxima and mean values for each optimization step (c). Finally, contributions of individual emission species (d) are determined for the trajectory and ten weather scenarios. The pareto fronts for each ensemble member serve as input for the aggregated results. From this set of ensembles, eight pareto-fronts show a similar correlation between relative changes of ATR and SOC, while in two cases we can observe 10% higher relative mitigation potential for the same SOCs, see Figure 36 (a). As already depicted in Figure 31, for the first ensemble of the 13th of June, there are almost no contrail-sensitive regions affecting the route. The mitigation potential in this case is dominated by the sensitivity to NO_x, specifically ozone, which can be addressed in order to reduce the relative climate impact up to 30% (see Figure 31.d). Water vapor and a small impact by contrails add another 3% of mitigation potential.

Example 2: Spanish Riviera (CG) – London (FG), 2018-06-18 0000 UTC (high contrail impact)

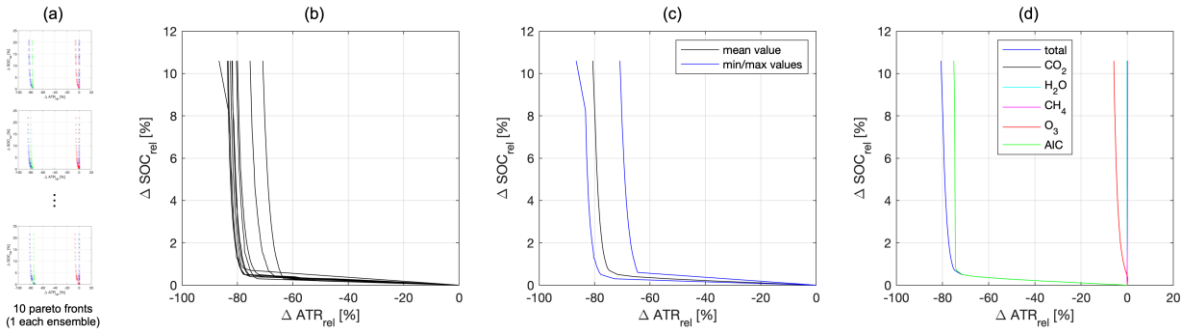

Figure 37. Probabilistic Pareto-fronts for the most relevant fictitious route. Individual Pareto-fronts (a) are aggregated (b) to evaluate minima, maxima and mean values for each optimization step (c). Finally,

EUROPEAN PARTNERSHIP
Co-funded by the European Union

contributions of individual emission species (d) are determined for the trajectory and ten weather scenarios of the 18th of June 2018.

The procedure to generate the pareto-fronts depicted in Figure 37 is identical, however we can observe a change in results. In this case all pareto front show a strong gradient at low cost penalties, because in all ensembles contrail sensitive regions could be avoided at low cost penalties (see previous section). This is due to the vertical deviation from the cost optimal route which has a low impact on the overall costs.

Sample shapes of the probabilistic pareto fronts

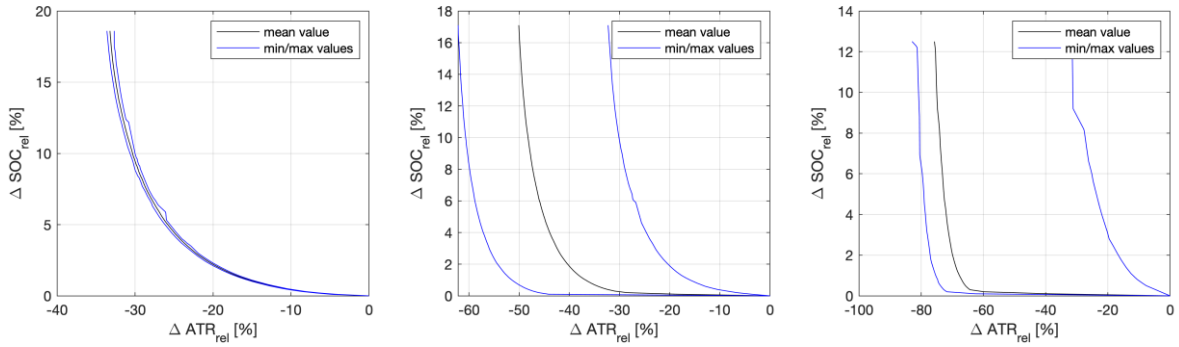

Figure 38. Individually sampled probabilistic pareto fronts for representation of weather variability and effects on eco-efficient trajectories.

To further understand the impact of the PES forecast ensembles on the mitigation potential we have analyzed individual routes to draw further conclusions. In Figure 38 samples of possible pareto-fronts are provided. There are three the main shapes identified when determining pareto-fronts for the set of ten ensembles:

- All ten ensemble paretos are very close to each other within an error margin of less than 5%, indicating very similar weather situations and consequently mitigation options when optimizing the trajectory (Figure 38,left).
- The ensemble paretos largely differ from each other – the maxima and minima in terms of relative ATR are far from the mean values. However, they are mostly equidistant to the mean, proving a forecast with lower precision but good accuracy (Figure 38,middle)
- Again a large discrepancy between minima and maxima is observed, however the mean value ist shifted towards either the maxima, or minima – indicating that a reduced number of individual members of pareto ensembles differ from the rest (Figure 38, right)

3.2.3 Mitigation potential

In this section more general conclusion are drawn from the optimization under consideration of forecast ensemble data. Furthermore, we aggregate results for the ten most relevant routes of our fictitious route network as a subset of data representative for the traffic scenario selected. We analyze the impact of atmospheric conditions on the solutions of our optimizations. We quantify the impact of weather and aCCFs over the selected months of summer (June) and winter (December) as well as day

EUROPEAN PARTNERSHIP
Co-funded by the European Union

and night-time effects. The aggregated results are shown by Pareto fronts and weighted by ASK of the fictitious route network.

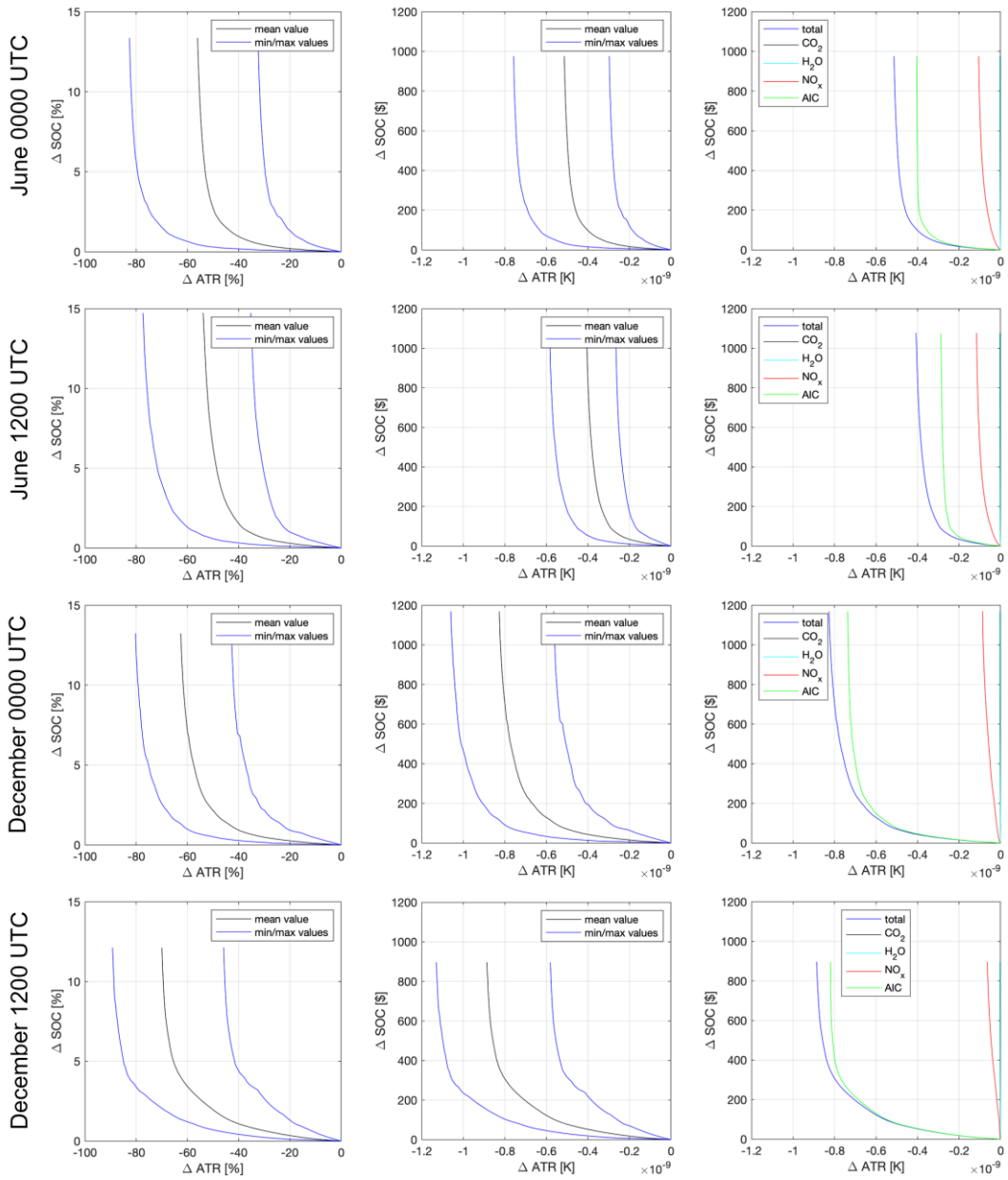

Figure 39: Aggregated pareto fronts of the Top 10 Routes of the fictitious route network scenario for December, 00:00 UTC. Relative pareto front including uncertainties (left), absolute pareto front including uncertainties (middle), absolute pareto front with contribution of individual species (right).

The ten most relevant routes from the fictitious route network account for an equivalent 100 real routes in terms of ASK. Similarly, to the procedure previously introduced in Example 1 of the single route analysis, we have calculated the mean values of the pareto front to generate aggregated results. In this instance absolute values are averaged values per trajectory. **In general, we observe large mitigation potential across both seasons and times**. By accepting increasing costs, we can achieve potentials of about 58% for day- and night-times in June. A strong gradient at low levels of relative SOC increase yield climate impact mitigation efficiencies of about 45% for a cost increase of 2%, see Figure

EUROPEAN PARTNERSHIP
Co-funded by the European Union

39. For the month of December, we observe higher total mitigation potentials of 61% and 70% for day-time and night-time respectively. The following table gives a simplified overview of the mitigation potential associated to SOC increases of 2,5 and 10%.

	Δ SOC			
Δ SOC	June 00:00 UTC	June 12:00 UTC	December 00:00 UTC	December 12:00 UTC
10%	55%	53%	62%	70%
5%	53%	48%	56%	65%
2%	46%	41%	45%	46%

Table 2: Total relative mitigation potential for summer and winter months at day- and night-time for given increases of relative SOC.

EUROPEAN PARTNERSHIP

Co-funded by the European Union

4 Summary and conclusion

This report presents achievements on the overall computation of environmentally-optimised trajectories using the Robust optimisation of structured airspace (ROOST) and Trajectory Optimisation Module (TOM) based on the air traffic sample of intra-ECAC flights in 2018 and the computed fictitious route network. An overview of the general simulation setup - including the implementation of aCCF's, meteorological data and traffic scenario – was given in D2.1 and is expanded in section 2 by more detailed information about constraints and boundaries applied to the optimisations for the integration of uncertainties.

Following the general setup, necessary changes and adaptations of cost functionals as well as further tool-specific constraints are described for both optimisation approaches in Sections 2.2.1 and 2.3.1 Moreover, this document presents exemplary results of individual routes to describe the applied methods and deliver an assessment on the robustness of environmentally-optimised trajectories. Overall mitigation potential is presented for the entire route network for each optimisation approach, followed by an intercomparison of the optimisation results again on the basis of single route examples.

The final results for the aggregated scenario are the following for ROOST:

- The mitigation potentials are highly variable due to changes in atmospheric conditions.
- For the considered case studies, in general, the night-time flights resulted in a higher reduction of climate impacts (≈ 20-50%) compared to day-time (≈ 20-30%).
- The mitigation potentials were mainly achieved by the reduction of the warming impact or increase of cooling impact of contrails.
- Overall, allowing a maximum 3% increase in cost could reduce the climate impact by 20-50% .
- The uncertainties on those results achieved by generating cooling contrails were high due to the tendency to fly through uncertain persistent contrail formation areas.

The final results for the aggregated scenario of TOM can be summarized as follows:

- The overall mitigation potential applying the continuous otpimization approach yields results in the order of 40-80%.
- The highest relative mitigation potentials come at a high increase of costs (often above 10%).
- For the investigated routes, as well as seasons and times, for a given increase of SOC we can observe mitigation potential variability across ensembles between 10 and 25% between best- and worst case scenarios.
- Higher absolut mitigation potentials could be achieved in the winter month.
- When contrails are present, the dominate the mitigation potential and generate strong gradients of mitigation potential at low cost increases.

EUROPEAN PARTNERSHIP

Co-funded by the European Union

5 References

[1] Bauer, P.; Thorpe, A.; Brunet, G.: The quiet revolution of numerical weather prediction, Nature, vol. 525, pp. 47–55, Sept. 2015.

[2] DuBois, D.; Paynter, G.: 'Fuel Flow Method 2' for Estimating Aircraft Emissions. In: Society of Automotive Engineers (SAE), SAE Technical Paper 2006-01-1987, 2006.

[3] Frömming, C., Grewe, V., Brinkop, S., Jöckel, P., Haslerud, A., Rosanka, S., . . . Matthes, S. (2020). Influence of the actual weather situation on non-CO_2 aviation climate effects: The REACT4C Climate Change Functions. Atmos. Chem. Phys., 21, 9151–9172, doi: 10.5194/acp-21-9151-2021

[4] González-Arribas, D., Andrés-Enderiz, E., Soler, M., Jardines, A., & Garcıa-Heras, J. Probabilistic 4D Flight Planning in Structured Airspaces through Parallelized Simulation on GPUs. In: International Conference for Research in Air Transportation (ICRAT) 2020.

[5] Grewe, V.; Dahlmann, K.; Flink, J.; Frömming, C.; Ghosh, R.; Gierens, K.; Heller, R.; Hendricks, J.; Jöckel, P.; Kaufmann, S.; Kölker, K.; Linke, F.; Luchkova, T.; Lührs, B.; Van Manen, J.; Matthes, S.; Minikin, A.; Niklaß, M.; Plohr, M.; Righi, M.; Rosanka, S.; Schmitt, A.; Schumann, U.; Terekhov, I.; Unterstrasser, S.; Vázquez-Navarro, M.; Voigt, C.; Wicke, K.; Yamashita, H.; Zahn, A.; Ziereis, H. Mitigating the Climate Impact from Aviation: Achievements and Results of the DLR WeCare Project. Aerospace 2017, 4, 34. https://doi.org/10.3390/aerospace4030034

[6] Grewe, V., Frömming, C., Matthes, S., Brinkop, S., Ponater, M., Dietmüller, S., . . . Hullah, P. (2014, 1).Aircraft routing with minimal climate impact: The REACT4C climate cost function modelling approach(V1.0).Geoscientific Model Development,7(1), 175–201. doi: 10.5194/gmd-7-175-2014

[7] Grewe, V., Matthes, S., Frömming, C., Brinkop, S., Jöckel, P., Gierens, K., . . . Shine, K. (2017, 2). Feasibility of climate-optimised air traffic routing for trans-Atlantic flights. Environmental Research Letters,12(3).doi: 10.1088/1748-9326/aa5ba0

[8] Jelinek, F.; Carlier, S.; Smith, J.: Advanced Emission Model (AEM3) v1.5 - Validation Report EEC Report EEC/SEE/2004/004, 2004.

[9] Lee, D. S., Fahey, D. W., Skowron, A., Allen, M. R., Burkhardt, U., Chen, Q., . . . Wilcox, L. J. (2021,1). The contribution of global aviation to anthropogenic climate forcing for 2000 to 2018.AtmosphericEnvironment,244. doi: 10.1016/j.atmosenv.2020.117834

[10] Lührs, Benjamin und Linke, Florian und Matthes, Sigrun und Grewe, Volker und Yin, Feijia (2021) Climate Impact Mitigation Potential of European Air Traffic in a Weather Situation with Strong Contrail Formation. Aerospace, 8 (50). Multidisciplinary Digital Publishing Institute (MDPI). doi: 10.3390/aerospace8020050 <https://doi.org/10.3390/aerospace8020050>. ISSN 2226-4310.

[11] Lührs, B.; Niklaß, M.; Frömming, C.; Grewe, V.; Gollnick, V.: Cost-Benefit Assessment of 2D and 3D Climate and Weather Optimized Trajectories. 16th AIAA Aviation Technology, Integration, and Operations Conference (ATIO), 13.-17. June 2016, Washington. DOI: 10.2514/6.2016-3758

[12] Mania, H.; Guy, A; Recht, B.: Simple random search of static linear policies is competitive for reinforcement learning. Advances in Neural Information Processing Systems, pp. 1800– 1809, 2018.

EUROPEAN PARTNERSHIP

Co-funded by the European Union

[13]Matthes, S., Lim, L., Burkhardt, U., Dahlmann, K., Dietmüller, S., Grewe, V., . . . Skowron, A. (2021). Mitigation of Non-CO_2 Aviation's Climate Impact by Changing Cruise Altitudes.Aerospace,8(2), 1–20.doi: 10.3390/aerospace8020036

[14]Matthes, S., Lührs, B., Dahlmann, K., Grewe, V., Linke, F., Yin, F., Shine, K. P. (2020, 11). Climate-optimized trajectories and robust mitigation potential: Flying atm4e.Aerospace,7(11), 1–15. doi:10.3390/aerospace7110156

[15]Nuic, A.; Mouillet, V.: User Manual fort the Base of Aircraft Data (BADA) Family 4. ECC Technical/Scientific Report No. 12/11/22-58, 2012.

[16]Patterson, M.A.; Rao, A.V.: GPOPS-II: A MATLAB Software for Solving Multiple-Phase Optimal Control Problems Using hp-Adaptive Gaussian Quadrature Collocation Methods and Sparse Nonlinear Programming. ACM Transactions on Mathematical Software, 41, 1-37, 2014.

[17]van Manen, J. & Grewe, V. (2019, 2). Algorithmic climate change functions for the use in eco-efficient flight planning. Transportation Research Part D: Transport and Environment,67, 388–405. doi:10.1016/j.trd.2018.12.016

[18]Wächter, A.; Biegler, L. T.: On the implementation of an interior-point filter line-search algorithm for large-scale nonlinear programming. In: Mathematical Programming 106, 25-57, 2006.

[19]Yin, F.; Grewe, V.; Castino, F.; Rao, P.; Matthes, S.; Yamashita, H.; Dahlmann, K.; Frömming, C.; Dietmüller, S.; Peter, P.; Klingaman, E.; Shine, K.P.; Lührs, B.; Linke, F.: Predicting the climate impact of aviation for en-route emissions: The algorithmic climate change function sub model ACCF 1.0 of EMAC 2.53. In preparation.

[20]Matthes, S.; Grewe, V.; Dahlmann, K.; Frömming, C.; Irvine, E.; Lim, L.; Linke, F.; Lührs, B.; Owen, B.; Shine, K.P.; et al. A Concept for Multi-Criteria Environmental Assessment of Aircraft Trajectories. Aerospace, 2017, 4, 42. doi:10.3390/aerospace4030042.

[21]González-Arribas, D., Jardines, A., Soler, M., García-Heras, J., & Andrés-Enderiz, E., . Probabilistic 4D Flight Planning in Structured Airspaces through Parallelized Simulation on GPUs. International Conference for Research in Air Transportation (ICRAT) 2020

[22]Simorgh A, Soler M, González-Arribas D, Matthes S, Grewe V, Dietmüller S, Baumann S, Yamashita H, Yin F, Castino F, Linke F. A Comprehensive Survey on Climate Optimal Aircraft Trajectory Planning. Aerospace. 2022 Mar 7;9(3):146.

[23]Simorgh, A. Soler, M., González-Arribas, D., Matthes, S., Grewe, V., Dietmüller, S., ... & Meuser, M. M. (2022). Robust 4D path planning in structured airspace for the benefit of environment using parallelized simulation on GPUs . Geoscientific Model Development (In preparation).

[24]Yamashita, H., Yin, F., Grewe, V., Jöckel, P., Matthes, S., Kern, B., ... & Frömming, C. (2020). Newly developed aircraft routing options for air traffic simulation in the chemistry–climate model EMAC 2.53: AirTraf 2.0. *Geoscientific Model Development*, *13*(10), 4869-4890.

EUROPEAN PARTNERSHIP

Co-funded by the European Union